UNITED STATES DEPARTMENT OF THE INTERIOR
OFFICE OF SURFACE MINING RECLAMATION AND ENFORCEMENT
APPLIED SCIENCE PROGRAM COOPERATIVE AGREEMENT

Development of a Modular Passive Treatment System and Evaluation of Reactive Substrates for Reducing Seasonal Effects of Acid Rock Drainage: Potential Application of Nanoparticles, Chelators, and Low Isoelectric Point Substrates

OSMRE: Idaho Acid Mine Drainage Cooperative Agreement, S17AC20000

FINAL TECHNICAL REPORT

Submitted by: Jeff Langman
Assistant Professor of Hydrogeology
Department of Geological Sciences

James Moberly
Associate Professor of Chemical Engineering
Department of Chemical & Materials Engineering

Wes Sandlin
Geology graduate student
Department of Geological Sciences

Research assistants: Thomas Thuneman and Michael Traver-Greene

Date: March 9, 2020

DISCLAIMER

ABSTRACT

Passive treatment systems were developed as lower-cost alternatives for remediation of poor-quality, mine drainage. Acidic drainage increases passive treatment difficulty because of greater metal concentrations and proton competition for reactive substrates. The goal of this project was to design an expandable, easily deployable, secondary treatment system to provide a flexible tool to reduce seasonal influent variation to a primary treatment system, improve overall treatment efficacy, and sustain/extend the life of the primary treatment system. A modular, passive, metal-removal system consisting of a series of insertable/removable cartridges contained in off-the-shelf, large-diameter PVC tubing (modular treatment system) was designed to expand to a desired contact time and contain reactive material that could be refreshed/replaced in situ. A range of substrates and surface modifications—including metal and silicate surfaces, metal and silica nanoparticles, and common chelators—were evaluated for potential use in the modular treatment system. Experimental results indicated that a functionalized, synthetic silica material (APTES-functionalized silica fiber (Si+APTES)) and a naturally-occurring silicate (zeolite) mineral (clinoptilolite) were viable reactive substrates for use in the modular treatment system. Permeability experiments indicate that clinoptilolite sustains a higher permeability than silica fiber. Batch sorption experiments using an iron-rich, acidic (pH of 3.0) solution indicate a specific sorption efficacy of Si+APTES > clinoptilolite > Si. Adsorption isotherms of the Si+APTES and clinoptilolite did not indicate a good fit with either the Langmuir and Freundlich adsorption models, which indicate additional metal capture processes not described by these models. Column experiment results indicate a sorption efficacy of clinoptilolite > Si+APTES for both small (10-cm length) and large (40-cm length) columns, which suggest increased metal sorption/removal by clinoptilolite given the column packing densities and flow conditions.

Clinoptilolite was selected for use as a reactive substrate during a field deployment of the modular treatment system prototype. Field deployment of the prototype yielded a flow rate of 4 L/min without obvious leaks or flow bypass. This flow rate was a result of a lack of hydraulic head rather than a lack of permeability in the reactive substrate. Iron removal was minimal in the field due to elevated seasonal acidity (pH of 2.5) that reduced the ability of the clinoptilolite to sorb metals (surface protonation). Further clinoptilolite sorption experiments over a pH range of 2.5 to 4.0 indicate substantial metal removal in solutions with a pH $\geq$ 3.0 and a decrease in iron removal from pH of 3.0 to 2.5 (no removal). Desorption experiments with ultrapure water, nickel-rich water, natural stream water, and iron-saturated clinoptilolite indicate that clinoptilolite retains sorbed iron at 5 ºC and 20 ºC under neutral (pH of 7.0) and mildly acidic (pH 4.0) conditions, but desorption of iron will occur at pH of 2.0. Overall, the modular treatment system can be readily deployed at relatively small seeps, adits, waste rock drainages with sufficient topographic gradient to provide hydraulic head to push the influent through the permeable reactive material. Clinoptilolite and Si+APTES have potential as reactive substrates for remediation in mildly acidic (pH $\geq$ 3.0) mine drainage under relatively higher (clinoptilolite) and lower flow (clinoptilolite or Si+APTES) conditions.

KEYWORDS: ARD passive treatment, metal sorption, clinoptilolite, APTES, nanoparticles

KEY ACRONYMS:

ARD: acid rock drainage

APTES: (3-aminopropyl)triethoxysilane [$C_9H_{23}NO_3Si$]

DO: dissolved oxygen

EtOH: ethanol

H^+: hydrogen ion/proton

mg/L: milligrams per liter

OH^-: hydroxide ion

PEI: branched polyethylenimine [$H(NHCH_2CH_2)_nNH_2$]

pH: H^+ concentration

pH_{pzc}: point of zero charge pH

PVC: polyvinyl chloride

rpm: revolutions per minute

Si fiber: a noncrystalline quartz (fused glass) consisting of fibers spun to 5 μm to 15 μm in diameter and woven into a wool form

Si+APTES: Si fiber coated with APTES

TABLE OF CONTENTS

LIST OF TABLES

LIST OF FIGURES

CHAPTER 1

INTRODUCTION

1.1 Background

Acid rock drainage (ARD) from the weathering of sulfidic ores and waste rock continues to significantly impact local and regional water resources across the United States and around the globe (Fig. 1.1) (Akcil & Koldas, 2006; Hedin et al., 1994; Moncur et al, 2014; Nordstrom, 2009). Abandoned mine sites with degrading infrastructure, unregulated mine water build-up, and discharge of ARD are acutely difficult sites for remediation. Common methods to address abandoned mine ARD are the restriction of potential discharge through mine dewatering (source control) or downstream collection of ARD for passive or active treatment (Hengen et al., 2014; Johnson & Hallberg, 2005). Passive and active treatment systems primarily target acidity reduction and associated metal mobility through chemical alteration. Passive systems are preferred because of lower costs of installation and operation (Egiebor & Oni, 2007; Johnson & Hallberg, 2005; Kefeni et al., 2017; Skousen et al., 2017). An ARD passive treatment system may be designed for a range of flow rates and metal concentrations, but large pulses of drainage and metals may induce higher rates of mineral precipitation and passivation of reactive surfaces, which can result in clogging or bypass of the treatment components (Hedin et al., 1994; Ludwig et al., 2002; McMahon et al., 1999; Puls et al., 1999; Skousen et al., 2017). Substantial surface passivation and bypass will reduce treatment efficacy and(or) shorten the life of a treatment system (Li et al., 2005; McMahon et al., 1999).

Figure 1.1: Example of acid rock drainage from Stockett, Montana, in the Great Falls Coal Field.

Mine site characteristics—including mineralogy, geomorphology, and biology—influence the weathering of sulfide minerals and the transport of oxidation products, but the hydrology of a site most directly affects the production of ARD through saturation of the weathering mineral surfaces with oxygenated water and flushing of solutes (Gozzard et al., 2011; Harris et al., 2003). Design and construction of passive treatment systems can be challenging for sites that experience periods of intense or extended rainfall and(or) snowmelt due to the associated large seasonal flux of discharge and metal concentrations (Gozzard et al., 2011; Hedin et al., 1994; Mayer et al., 2006; Moncur et al., 2014; Nordstrom, 2009). Strong seasonal differences can make it difficult to estimate representative discharges or metal concentrations, leading to incorrect design of the primary treatment system (Costello, 2003). Under or over design of the system can shorten the lifespan or significantly increase remediation costs (Costello, 2003).

The most common factors leading to passive treatment system failure are surface passivation of reactive material and flow bypass. Metal sorption and(or) mineral precipitation within a treatment system will reduce surface reactivity and ultimately determine the life of the system (Alcolea et al., 2012; Costello, 2003; Kruse et al., 2012; Obiri-Nyarko et al., 2014; Santomartino & Webb, 2007; Skousen et al., 2017; Watzlaf et al., 2000). Sorbed elements/compounds and precipitates can occur in various forms depending on acidity and reduction-oxidation (redox) conditions that influence metal forms/species and solubility (Lee & Wilkin, 2010; Santomartino & Webb, 2007; Watzlaf et al., 2000; Ziemkiewicz et al., 1997). As sorbed metals and mineral precipitates reduce reactive surface availability (Fig. 1.2), treatment efficacy is reduced unless additional reactive surface is available in the transport pathway(s) (Kruse et al., 2012; Santomartino & Webb, 2007). The accumulation of precipitates and microbial biomass also reduce permeability, alter flowpaths, and reduce residence/contact time necessary for the desired reactions to occur (Fig. 1.3) (Baker & Banfield, 2003; Costello, 2003; Gibert et al., 2013; Lee & Wilkin, 2010; Li et al., 2005; McMahon et al., 1999; Skousen & Ziemkiewicz, 2005). The predicted life of a passive treatment system is based on the exhaustion of all available reactive surfaces, but system life can be difficult to estimate because of seasonality of discharge and metal concentrations (Obiri-Nyarko et al., 2014; Skousen et al., 2017).

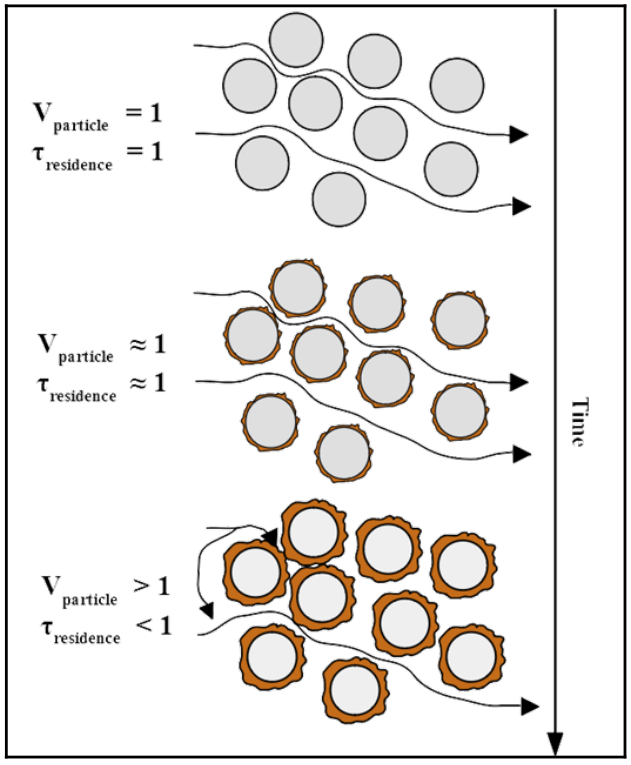

Figure 1.2: Sorption of metal ions on a sorbing surface, which limits surface availability.

The inability of passive treatment systems to adjust to changes in discharge and metal concentrations can limit their application in comparison to active treatment systems (Johnson & Hallberg, 2005). Instead of designing a singular system for passive treatment of ARD, remediation managers are examining multi-component systems (Costello, 2003; Johnson & Hallberg, 2005; Kepler & McCleary, 1993). These complimentary systems can assist in reducing acid, metal, and sulfate [SO_4] concentrations, and variable discharge rates can be spatially integrated with modular systems in relatively small footprints. A modular and expandable design within individual systems can provide additional flexibility to assist with construction/deployment as mine drainage evolves. Flexibility of design, particularly a modular design that allows for refreshing of a treatment material, can reduce the impact of seasonal flux of discharge and metal concentrations, increase treatment efficacy, extend overall system life, decrease costs, and minimize ARD environmental impacts.

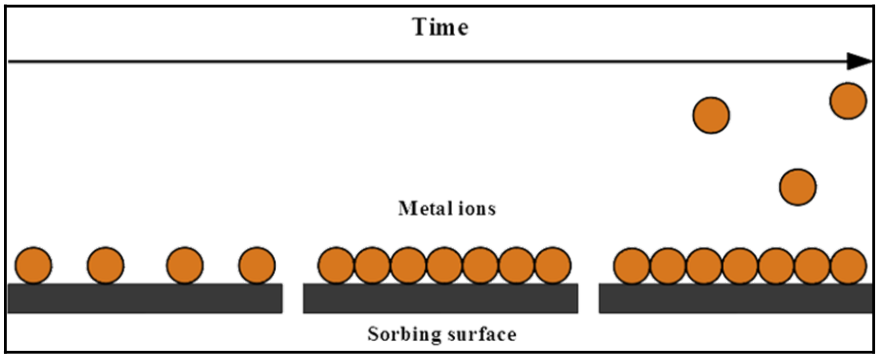

Figure 1.3: Accumulation of precipitates on reactive materials resulting in preferential flowpaths and decreased contact. $\mathbf{V}_{particle}$ = particle velocity; $\boldsymbol{\tau}_{residence}$ = residence time.

1.2 Objectives

For this study, an interdisciplinary research team from the University of Idaho designed and constructed a modular, flexible, passive metal removal system (modular treatment system) to be placed upstream of, and used in conjunction with, a primary treatment system for remediation of ARD. Laboratory experiments were conducted with potential substrates and surface modifications for metal removal by sorption/precipitation leading to a field deployable prototype. This report provides a blueprint for the construction and deployment of the modular treatment system, a comparison of potential reactive substrates for remediation of ARD, and an examination of the effects of pH on the sorption and retention (desorption) of iron [Fe] on silicate surfaces.

Following are the project objectives:

- Design a low-cost, modular and expandable treatment system that can incorporate one or more reactive substrates and can be refreshed without removal of the treatment system.
- Conduct laboratory experiments on a range of substrates and surface modifications, including metal and silicate surfaces, metal/silica nanoparticles, and common chelators to determine their utility for remediation of ARD.
- Select the highest performing substrates and surface modifications for detailed sorption analysis.
- Select a reactive substrate/surface modification for use in a prototype and monitor its performance in a multi-day field deployment.

CHAPTER 2

MODULAR TREATMENT SYSTEM DESIGN

2.1 Modular treatment system

The modular treatment system was designed as a modular, flexible device intended to be deployed upstream of a primary treatment system(s) (final design shown in Fig. 2.1). All materials selected for the modular treatment system are corrosion resistant and can withstand the high acidity of ARD. The physical design consists of three components: an entry weir that directs drainage into the system, an outer framework composed of individual pipe/elbow units, and reactive material cartridges that are inserted into each unit of the outer framework (Figs. 2.1 and 2.2). The cartridges can be filled with a choice of reactive material(s). Any cartridge can be removed, refreshed with new reactive material, and reinstalled through removal of a unit's top cap (PVC elbow). The modular design of the system allows additional units (cartridges) to be added to the system in order to reach a desired residence/contact time. Additionally, unit elbows can be positioned at various angles so that the modular treatment system expands or contracts to fit a desired space or hillslope. The system is designed to be partially buried next to the drainage where ARD is routed into the system, exits the final unit, and drains back into the channel. The partial burial of the system provides stability and allows top elbows to be removed for cartridge removal/insertion. Each segment of the system is slightly lower than the previous segment (outer framework tube extension at each successive cartridge location) so that a hydraulic gradient will push influent through the system. The cost of materials for a modular treatment system with six cartridges (excluding reactive material) is $3,831 as of November 2019 (Table 2.1).

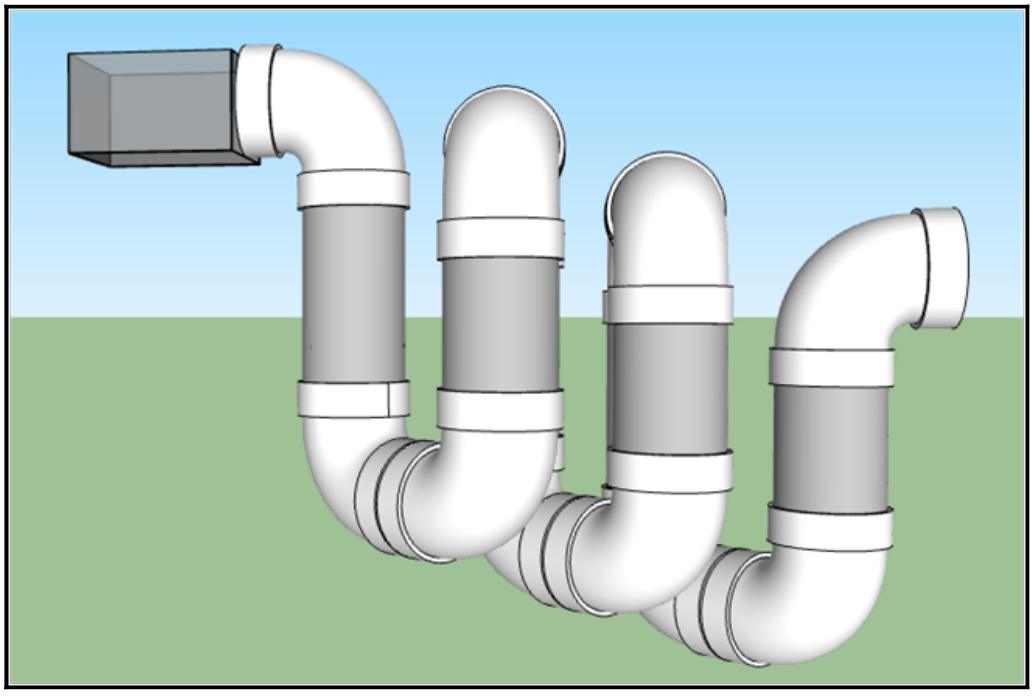

Figure 2.1: Modular treatment system entry weir (gray box) and outer framework for a six-cartridge configuration.

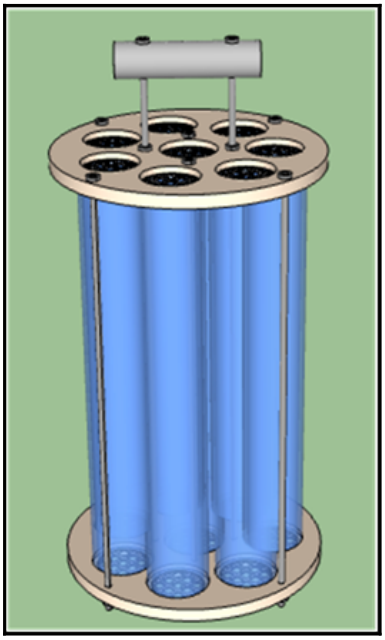

Figure 2.2: Cartridge for modular treatment system. Individual tubes are filled with reactive material of choice.

2.2 Entry weir

The entry weir was constructed by cutting a 20 cm (base) × 10 cm (height) v-notch into a polypropylene container (Fig. 2.3). Cuts were made at 45º angles from the top edge of the container. PVC sheet stock was cut into a semicircle (1-cm thick × 25-cm diameter) and glued to the entry tube to prevent backflow. The entry weir is designed to be partially buried so that drainage flows into the weir from the opposite end of the v-notch, exits the v-notch over the semicircle, and flows into modular treatment system.

Table 2.1: Materials and costs for a 6-cartridge, modular treatment system.

Category	Part name	Company	Price ($)
Entry weir	Polypropylene drawer	Sterilite	$3.65
Unit cartridge	Sheet stock, PVC Type 1, 12"W × 12"L × 0.5"	Grainger	$217.75
Outer framework	10" Sch. 40 PVC Pipe	PVC Fittings Online	$322.60
Outer framework	10" Sch. 40 PVC 90 Elbow Soc.	PVC Fittings Online	$2,443.92
cartridge	2" Sch. 40 PVC Pipe	PVC Fittings Online	$116.00
cartridge	¼" Stainless Steel Threaded Rods	Grainger	$179.20
cartridge	1"D Multipurpose 6061 Aluminum	McMaster-Carr	$16.85
cartridge	Chemical-Resistant Viton Fluoroelastomer O-Ring	McMaster-Carr	$22.35
cartridge	2"D PVC Snap-In Drain Insert	Oatey	$412.80
cartridge	18-8 Stainless Steel Hex Nut (¼")	McMaster-Carr	$5.36
cartridge	Fluorosilicone Rubber Sealing Washer (¼")	McMaster-Carr	$90.40
		TOTAL:	$3,830.88

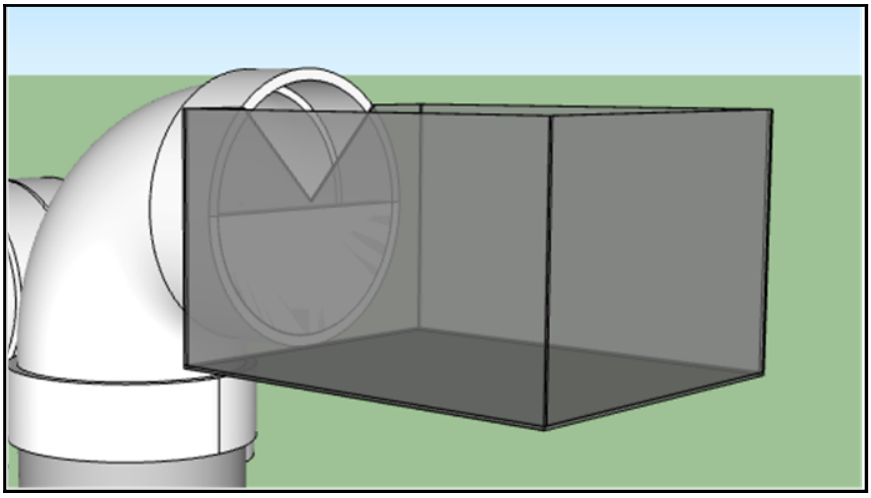

Figure 2.3: Entry weir with v-notch that directs drainage over semicircle sheet stock and into modular treatment system.

2.3 Outer framework

The outer framework consists of Schedule 40 PVC tubing (25-cm diameter) connected by 90º elbows (Fig. 2.4). Elbows were connected to each other with segments of the PVC tubing (33-cm length). Vertical units of PVC were cut to lengths of 61 and 46 cm (3 each) and connected in an alternating series that creates a stair-step configuration that provides a hydraulic gradient. The number, spacing, orientation, and stair-step drop of units can be adjusted depending on space, desired number of cartridges (contact time), and needed hydraulic gradient for the influent volume. The outer framework is designed to be partially buried in a hillslope for stability, with the bottom of the entry elbow just above the ground surface.

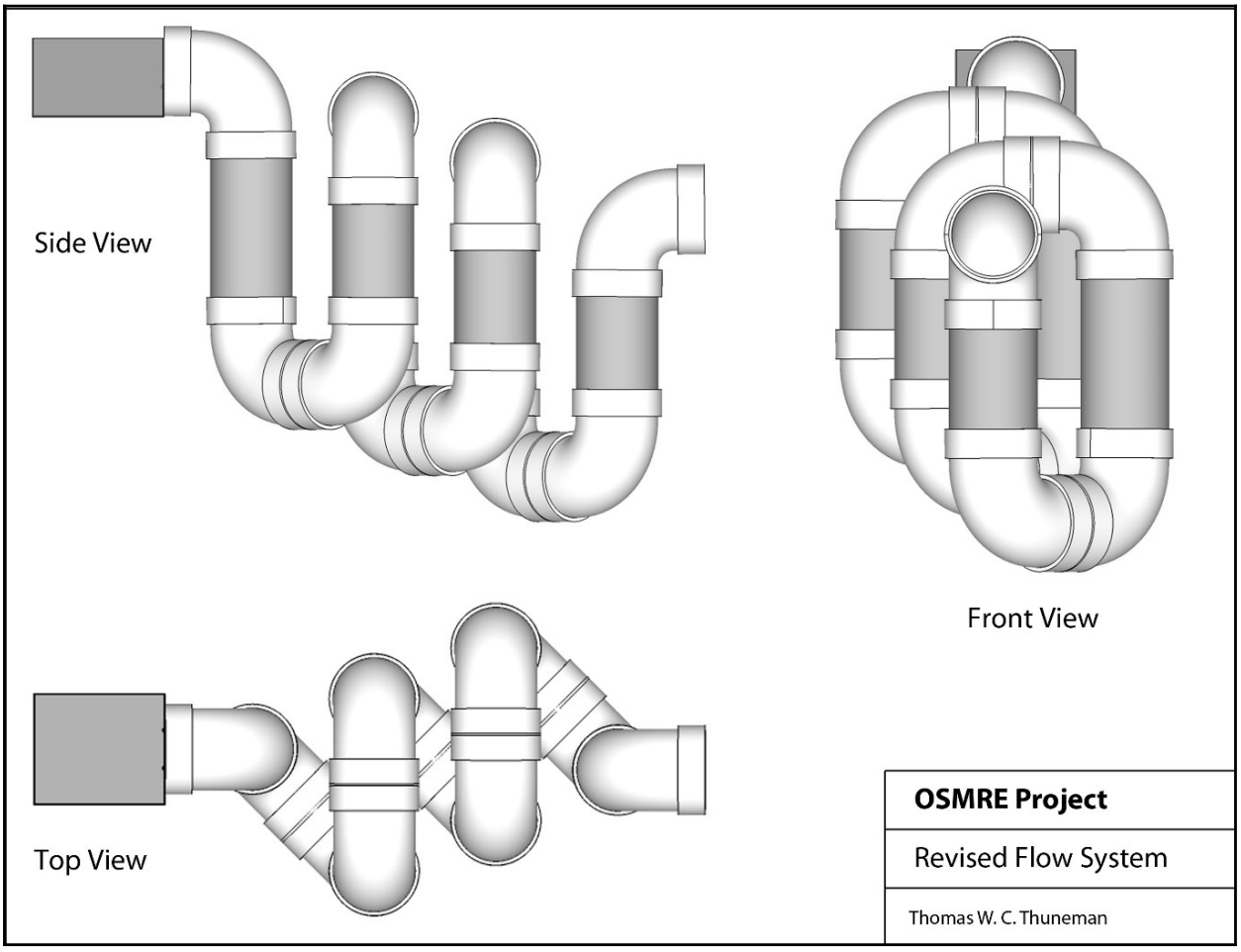

Figure 2.4: Outer framework of treatment system. Drainage enters through the weir (gray box) where hydraulic head pushes drainage through each cartridge unit (gray tubes).

2.4 Cartridges

A cartridge consists of eight Schedule 40 PVC tubes (41-cm length × 5-cm diameter), two Schedule 40 PVC sheet stock (1-cm thick × 25-cm diameter), six stainless steel threaded rods (46-cm length × 0.6-cm diameter), two stainless steel threaded rods (53-cm length × 0.6-cm diameter), one corrosion resistant aluminum rod handle (13-cm length × 2.5-cm diameter),

sixteen PVC snap-in drains (5-cm diameter), two Viton O-rings (0.26-cm width × 24-cm inner diameter), twenty stainless steel hex nuts (0.6 cm), and sixteen fluorosilicone rubber washers (0.6 cm) (Fig. 2.5). Sheet stock was lathed to the dimensions shown in Figure 2.5. Eight holes (0.6-cm diameter) were drilled into the sheet stock where threaded rods were inserted. Four of these holes were drilled 4 cm from the center of the sheet stock and the other 4 holes were placed 11.7 cm from the center of the sheet stock (Fig. 2.5). Eight additional holes were drilled into the sheet stock for the PVC tubes. Each of these holes have a blind hole (6-cm diameter) drilled to a depth of 0.6 cm, with an inner hole (5.4-cm diameter) drilled through the sheet stock (Fig. 2.5). One of these holes is located at the center of the sheet stock with the other 7 holes located 7.8 cm from the center of the middle hole, separated by angles of 51.4º. Snap-in drains were glued in these holes. A seal groove (0.26 cm width × 0.2-cm depth) was lathed into the outer perimeter of the sheet stock where O-rings were placed to provide a seal between the cartridge and the outer framework (Fig. 2.6). Finally, two 0.6-cm holes were drilled through the aluminum rod handle 7.9 cm apart (2.5 cm from the ends of the rod) to allow for removal of the cartridge.

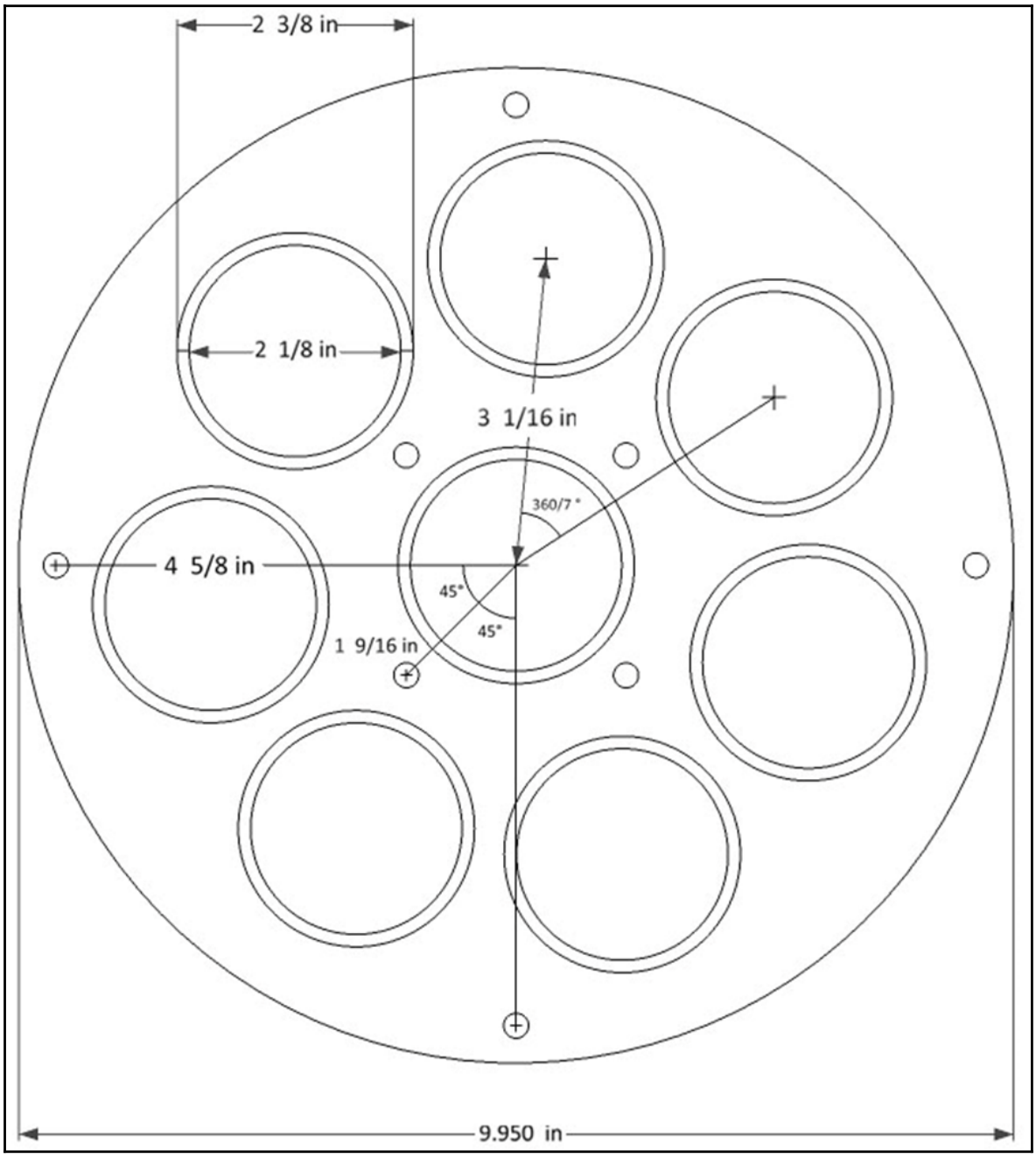

Figure 2.5: Diagram of sheet stock with cartridge openings dimensions for cartridges (units = inches).

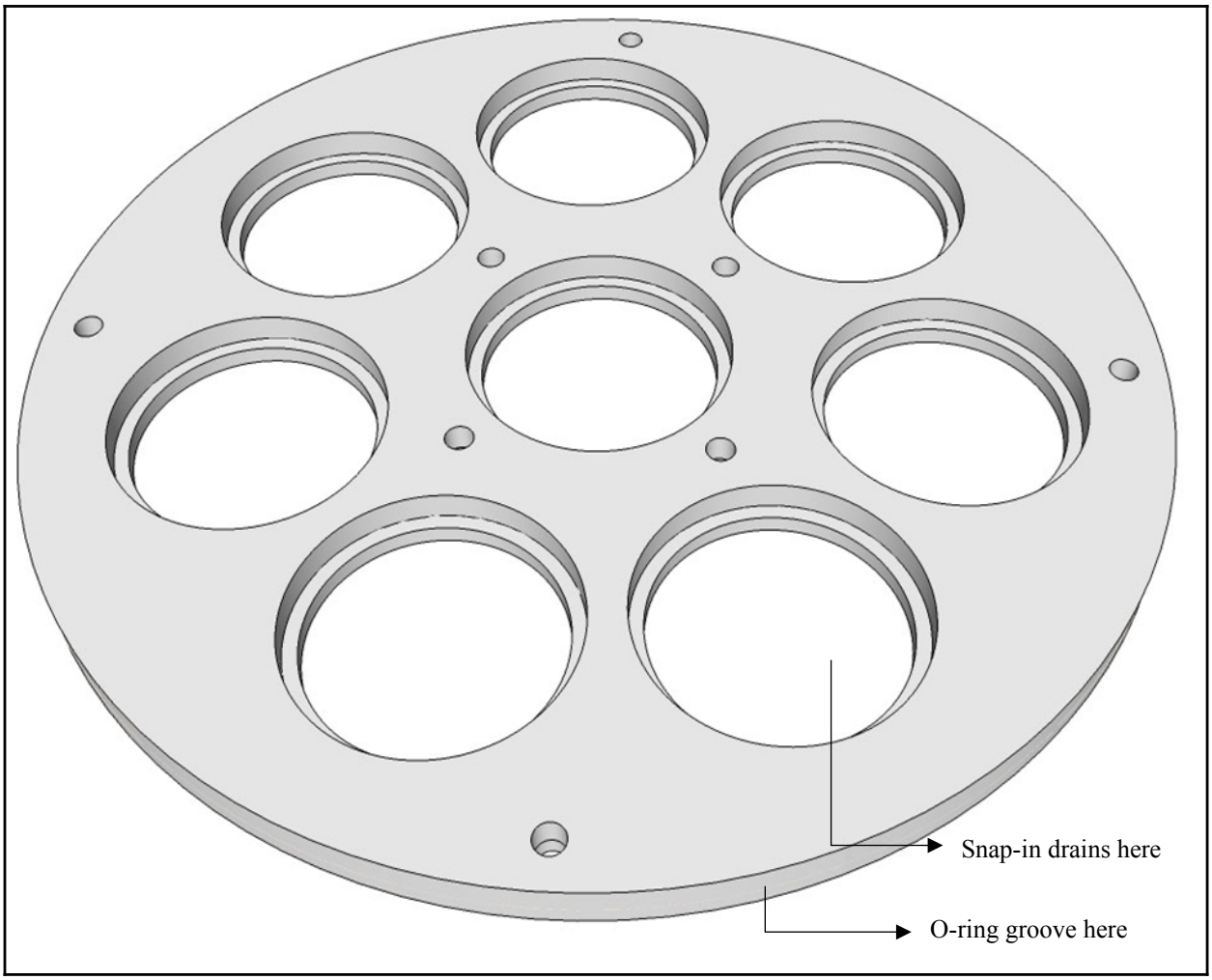

Figure 2.6: Projection of PVC sheet stock lathed for cartridge insertion. O-ring groove not shown in the figure.

To assemble a cartridge (Fig. 2.7), PVC tubes were inserted so that one end fit between the sheet stock and the snap-in drains, pressing firmly against the inner blind-hole. At this point, reactive material can be inserted into the individual PVC tubes. The other sheet stock was then fit to the opposite end of the PVC tubes. To stabilize the cartridge, six threaded rods (46-cm length) were inserted through the drill holes and secured with hex nuts and rubber washers. Two of the threaded rods were longer than the remaining rods (53-cm length) to allow the aluminum rod handle to be secured to the top of the cartridge (Fig. 2.8). Finally, Viton O-rings were inserted along the outer groove of the sheet stock. The cartridges and outer framework tubes were lubricated with Plumber's Grease (Oatey®) for easy insertion, alteration of orientation, sealing of O-rings, and easy removal.

Figure 2.7: Assembled cartridges—A) clear PVC tubes filled with clinoptilolite, B) standard white PVC tubes.

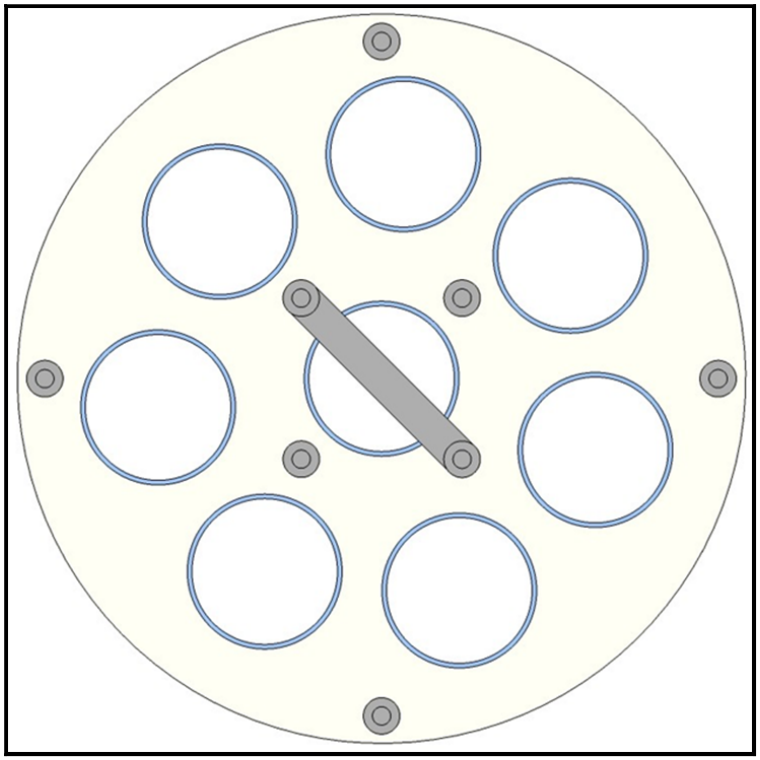

Figure 2.8: Top view of cartridge showing placement of aluminum rod handle.

CHAPTER 3

SUBSTRATE COMPARISON AND SELECTION

3.1 Introduction

Quality of mine drainage typically is proportional to the acidity of the drainage (Kefeni et al., 2017; Nordstrom, 2009). The most common metal sulfide and cause of ARD is the oxidation of pyrite [FeS_2] (Akcil & Koldas, 2006), and the release and solubility of Fe and other metal contaminants is a product of the resulting acidity (Bigham & Nordstrom, 2000; Dold, 2017; Egiebor & Oni, 2007; Nordstrom, 2011; Nordstrom et al., 2015). The design and construction of passive treatment systems can be challenging for sites that experience large seasonal flux of Fe concentrations and environmental conditions (August et al., 2002; Brooks et al., 2001; Gozzard et al., 2011; Mayer et al., 2006; Moncur et al., 2014; Nordstrom et al., 2015). The form of Fe in ARD and its capture by treatment (reactive) substrates depends on the balance of protons [H^+], dissolved oxygen (DO), and associated cations and anions (e.g., commonly associated metals such as nickel [Ni] and oxidized sulfur compounds such as sulfate [SO_4]) (Nordstrom, 2009; Nordstrom et al., 2015).

Passive treatment of poor-quality mine drainage includes the use of biological, geochemical, and physical processes to improve water quality (Skousen et al., 2017). Reactive inorganic or organic materials, such as calcite or organic waste, induce metal capture through alteration of environmental conditions (pH or reduction-oxidation potential) (Gibert et al., 2004; Skousen et al., 2017). Passive removal of metals through sorption on inorganic substrates can be viewed as the interaction of a solution cation and an oxide surface (Davis & Leckie, 1978; Dzombak & Morel, 1990; Stumm & Morgan, 1996). The electrostatic interaction between metal ions and a charged surface (commonly the oxide of another metal) provide a treatment option for the removal of metals from solution (Gibbs free energy of sorption), which is influenced by surface site characteristics and ions-in-solution competition (Stumm & Morgan, 1996).

For this investigation, various substrates (sorbing surface) and surface modifications (metal capture enhancement) were evaluated for creation of a reactive substrate for insertion into the modular treatment system. The goal was to provide options for possible substrates that could be readily purchased and modified with potential ease of insertion/removal into/from the modular treatment system. The focus of the substrate evaluation was selection of low isoelectric point substrates that would capture Fe and other metals from solution through sorption or other secondary processes (e.g., mineral precipitation). Secondary processes of mineral precipitation and/or alteration of solution pH were not primary objectives of the substrate selection but provide additional metal capture properties that are composited into the overall evaluation of Fe removal from solution. Substrates—including steel plates, tungsten wire, silica felt/wool, and a natural silicate mineral (zeolite)—and multiple surface modifications—including metal nanoparticles, silica nanoparticles, mesoporous silica microparticles, and various common chelators—were evaluated for potential use in the modular treatment system. Experimental

results indicated that a manufactured, silica material (silica (Si) fiber) with chelator (APTES-functionalized Si fiber (Si+APTES)) and a zeolite mineral (clinoptilolite) were viable reactive substrates for use in the modular treatment system. A review of all tested substrates and surface modifications is presented in Appendix A.

The primary influence of pH on the solubility of metals is due to the presence of competing protons (Dzombak & Morel, 1990; Heidmann et al., 2005), which is represented by the point of zero charge (pH_{pzc})—a proton concentration (pH) sufficient to neutralize the residual negative surface charge that allows sorption to occur (Nelson et al., 2019). The interaction between H^+ and OH^- surface groups provides competition for sorption of metals where sufficient H^+ activity leads to the isoelectric point through full protonation of the surface (Parks, 1967). Artificial and natural silicate and aluminosilicate substrates such as fused quartz (silica glass) and zeolite minerals tend to have a pH_{pzc} near 3.0 (Cotton, 2008; Gainer, 1993), which makes such substrates applicable to ARD treatment for weak (≥4.5 pH) to mildly (≥3.0) acidic solutions. Metal capture by sorption on silicate substrates (e.g., zeolites and clays) is common for treatment of waste water (Faghihian et al., 1999; Pandová et al., 2018; Yavuz et al., 2003), but few silicate options are currently known to be effective for sorption of metals in ARD. A final selection of Si+APTES and clinoptilolite [$(Na,K,Ca)_{2-3}Al_3(Al,Si)_2Si_{13}O_{36}\cdot 12H_2O$] were chosen for sorption testing because of their ease of purchase, simplicity of handling and surface preparation, permeability, large surface areas, and ability to sorb and retain metals during submersion in acidic solutions in comparison to the other evaluated substrates and surface modifications.

3.2 Materials and methods

The selected silica fiber, obtained from Technical Glass Products, is a noncrystalline quartz (fused glass thread = Si fiber) consisting of fibers spun to 5 μm to 15 μm in diameter and woven into a felt/wool form. Specific surface area was calculated based on the assumption that the Si fiber is constructed by a continuous cylindrical fiber averaging 10 μm in diameter. Given a specific volume of 0.45 cm^3/g for fused glass, a total length (height (h) of continuous fiber) of 5,787 m/g for the given volume, a specific surface area (A) of 18 m^2/g can be calculated from:

$$h = \frac{V}{\pi r^2} \tag{1}$$

$$A = 2\pi rh + 2\pi r^2 \tag{2}$$

The Si fiber is coated (front and back) with a starch binder for ease of handling (Fig. 3.1). The weaving of the fiber provides torsion and bending resistance in a flexible wool that may be manipulated (e.g., rolled, packed) to provide structural resistance to the flow of water.

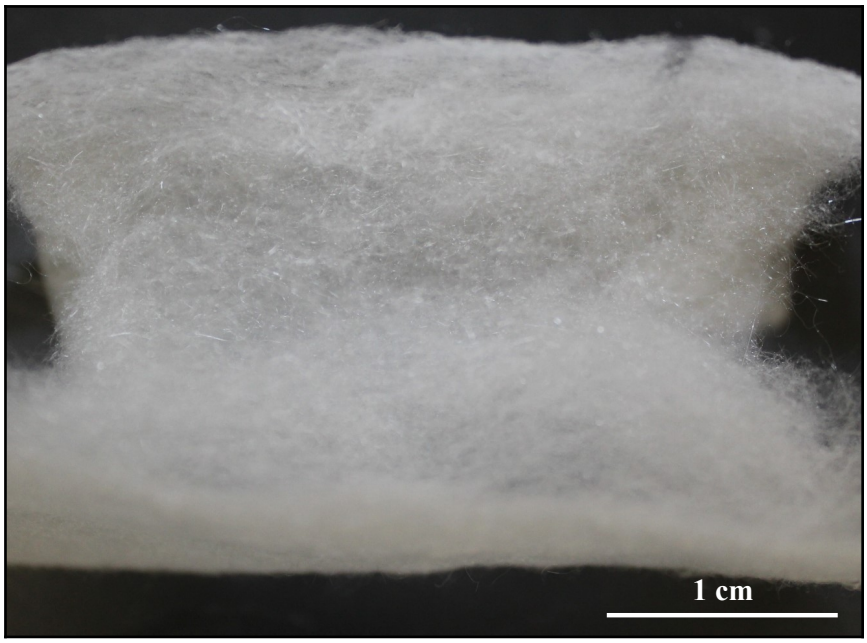

Figure 3.1: Silica fiber spun into a felt with a starch coating on top and bottom.

Clinoptilolite is a natural zeolite mineral ([hydrated $(Na,K,Ca)_{2\text{-}6}Al_xSi_yO_z$]), which are micro-porous aluminosilicates with large surface areas (Burakov et al., 2018; Pandová et al., 2018). Metals can be captured by zeolites through sorption as well as cation exchange, in which alkali/alkaline metals located within zeolite are replaced by cations in solution (Holub et al., 2013; Motsi et al., 2009; Pandová et al., 2018; Stylianou et al., 2007; Wang & Peng, 2010). For this study, clinoptilolite was obtained from KMI Zeolite, Inc. (Nevada). The clinoptilolite grains ranged from 2.4 to 4.8 mm in diameter (4 × 8 mesh) (Fig. 3.2). Specific surface area was determined by the manufacturer to be 40 m^2/g. Clinoptilolite samples were triple-rinsed with reverse-osmosis filtered water (ultrapure water) and dehydrated (24 hrs at 80 ºC) prior to experimental use to remove clinoptilolite dust generated during mining and handling.

Figure 3.2: Clinoptilolite grains, 4 × 8 mesh.

3.2.1 Column substrate permeability

The bare Si fiber and clinoptilolite were evaluated for permeability when packed into 5-cm diameter columns. Permeability experiments were conducted by filling clear PVC columns (5-cm diameter × 40-cm length) with Si fiber or clinoptilolite (Fig. 3.3). Bare Si fiber was tightly rolled and inserted into the column perpendicular to the rolling direction. This configuration allows structural resistance against collapse

under high flow. Multiple packing arrangements of the Si fiber were evaluated, and the rolled configuration provided the greatest structural integrity along with highest possible surface area density. Packing densities of 0.073, 0.037, and 0.018 g/cm^3 were tested in the rolled configuration.

Clinoptilolite was poured into the column until grains were freely settled with handling, reaching a packing density of 0.73 g/cm^3. Hydrostatic pressure directed water from a 57-L container through the flow column and into a separate container where the effluent flow rate was measured with a 1-L beaker and stopwatch. Flow measurement occurred after 1 min of flow through the column to allow for full saturation and settling of the substrate. A constant head of 34 L was maintained throughout the experiment with a peristaltic pump that recirculated water from the lower to upper tank. A dye tracer was included in the permeability test solutions to evaluate any preferential flow or bypass occurring in the column.

Figure 3.3: Experimental setup for permeability experiments.

3.2.2 *Si fiber functionalization*

The Si fiber can be functionalized with a chelator through silanization where ethoxy groups hydrolyze and form covalent Si-O-Si bonds (Liu et al., 2013). A review of possible chelators for functionalization with the Si fiber (or clinoptilolite) resulted in branched Polyethylenimine [$H(NHCH_2CH_2)_nNH_2$] (PEI) and (3-Aminopropyl)triethoxysilane [$C_9H_{23}NO_3Si$] (APTES) being tested for potential use as chelators in preliminary experiments. APTES was the final selection for surface functionalization of the Si fiber due to its ease of silanization, low viscosity, superior surface coverage, and ability to capture metals through amine functional groups that have shown application for metal capture in a variety of solutions (Barquist, 2009; Ramasamy et al., 2017; Ramasamy et al., 2018). APTES was applied to the Si fiber per methods developed by Acres et al. (2012) and Liu et al. (2013). The desired amount of Si fiber was submerged in a 2% APTES (98% EtOH) solution for 20 min while agitated on an orbital shaker. Following submergence, the Si+APTES was removed and repeatedly rinsed with 100% EtOH and ultrapure water. Rinsed Si+APTES were dried in an oven at 80 ºC for 15 hr. Si surfaces were not treated with an oxidizer, such as piranha solution (mixture of sulfuric acid [H_2SO_4] and hydrogen peroxide [H_2O_2]), prior to functionalization (Acres et al., 2012; Zhu et al., 2012) because such a step would have removed the starch coating that is crucial to its structural integrity.

3.2.3 *Preparation of acidic Fe^{2+} solutions*

Acidic Fe^{2+} solutions were prepared for sorption experiments at Fe concentrations of 25 to 1,000 mg/L by dissolving an appropriate mass of ferrous-sulfate heptahydrate [$FeSO_4 \cdot 7H_2O$] in ultrapure water. H_2SO_4 was added to each solution until a pH of 3.0 was obtained and stable while the solution was mixed on an orbital shaker at 100 rpm for 30 min.

3.2.4 *Batch sorption experiments*

Batch sorption experiments were conducted on equivalent surface areas (216 m^2) of each substrate by inserting 12 g of Si, 12 g of Si+APTES, and 5.4 g of clinoptilolite within polyester mesh bags in triplicate and suspending them in acidic Fe^{2+} solutions [25, 50, 75, 100 mg/L] at 20 ºC. Solutions were continuously agitated on an orbital shaker at 100 rpm, and a pH of 3.0 ± 0.1 was maintained through introduction of H_2SO_4 for the duration of the experiments. Solution samples were collected at the start and end of the experiment and analyzed for total Fe concentration with a Hach 3900 spectrophotometer and FerroVer reagent. Quality control and accuracy were checked with instrument blanks, replicate samples, and calibration standards over the course of the study. Such quality control measures also were instituted for the small-scale and large-scale flow-through column experiments. No false positive results were reported, and replicate results were within acceptable range for Fe concentration. Specific sorption values (q; mg/g) were calculated using:

$$q = \frac{C_i - C_f}{M} \tag{3}$$

where C_i and C_f are initial and final solution concentrations of Fe, respectively, and M is substrate mass.

3.2.5 Adsorption isotherms

The specific sorption values for each substrate were compared to Langmuir and Freundlich isotherm models. The Langmuir isotherm model assumes a homogeneous surface with a finite number of monolayer sorption sites (Langmuir, 1918):

$$q_e = q_{max} \frac{K_L C_e}{1 + K_L C_e} \tag{4}$$

where q_e is amount adsorbed at an equilibrium concentration C_e, q_{max} is maximum monolayer adsorption, and K_L is the Langmuir constant related to free energy of adsorption (Holub et al., 2013). The Freundlich isotherm model assumes a heterogeneous surface where adsorption can occur in multiple layers (Erdem et al., 2004; Holub et al., 2013; Limousin et al., 2007):

$$q_e = K_f C_e^{1/n} \tag{5}$$

where K_f is the Freundlich constant related to maximum adsorption capacity and n is a constant related to adsorption intensity (Fan & Zhang, 2018; Holub et al., 2013).

3.2.6 Small-scale column experiments

Small-scale column experiments were conducted by inserting 15 g of Si+APTES or 150 g of clinoptilolite (packing densities of 0.073 and 0.73 g/cm^3, respectively) within a clear, PVC column of 5-cm diameter × 10-cm length (Fig. 3.4). Si+APTES was tightly rolled into a cylinder form prior to insertion into the column to provide sufficient structural integrity during wetting and maximize surface area availability. A peristaltic pump directed acidic (pH of 3.0) Fe^{2+} solution (1,000 mg/L) to the bottom of the flow column, through the permeable substrates, out the top of the column, and into a separate container at a rate of 25 mL/min and 12 mL/min for Si+APTES and clinoptilolite, respectively. Flow rates were determined for the substrates based on packing density such that the initial effluent exited the flow columns after equivalent residence times of 7.5 min. Effluent solution was collected at 0, 7.5, 15, 30, 60, 90, 120, 150, 180, 240, 300, and 360 min. Total Fe concentration was measured with a Hach DR3900 spectrophotometer until Fe saturation of each substrate (outflow Fe concentration of 1,000 mg/L). Three replicate, small-scale column experiments for each substrate were conducted in sequential order. Following each experiment, the column apparatus was cleaned in a 15% nitric acid [HNO_3] bath and rinsed with ultrapure water.

In both small- and large-scale column experiments, the concentration of removed Fe was found by subtracting effluent Fe concentration from influent Fe concentration. The area under the breakthrough curve attained by integrating the removed concentration (C_{rem}; mg/L) versus time (min) plot can be used to find the total Fe removed (R_{total}; mg) in the column for a given pumping rate (Q) (Aksu & Gönen, 2004).

$$R_{total} = \frac{Q}{1000} \int_{t=0}^{t=t_{total}} C_{rem}\, dt \tag{6}$$

Figure 3.4: Example of small-scale column experiment.

3.2.7 Large-scale column experiments

Large-scale column experiments were conducted by inserting 600 g of clinoptilolite (0.73 g/cm^3 packing density) within a clear, PVC column of 5-cm diameter × 40-cm length (Fig. 3.5). A peristaltic pump directed acidic (pH of 3.0) Fe^{2+} solution (1,000 mg/L) to the bottom of the flow column, through the permeable substrate, and into a separate container at a rate of 12 mL/min. Effluent solution was collected at 0, 0.5, 0.75, 1, 1.5, 2, 4, 6, 8, 14, 20, 26, 32, 38, 44, 50, 56, 62, 68, 74, 80, 86, 92, 98, and 104 hr. Total Fe concentration was measured with a Hach DR3900 spectrophotometer until saturation of the clinoptilolite. Large-scale column experiments were similarly conducted in triplicate. Total Fe removed during these experiments were calculated according to Eq. 6.

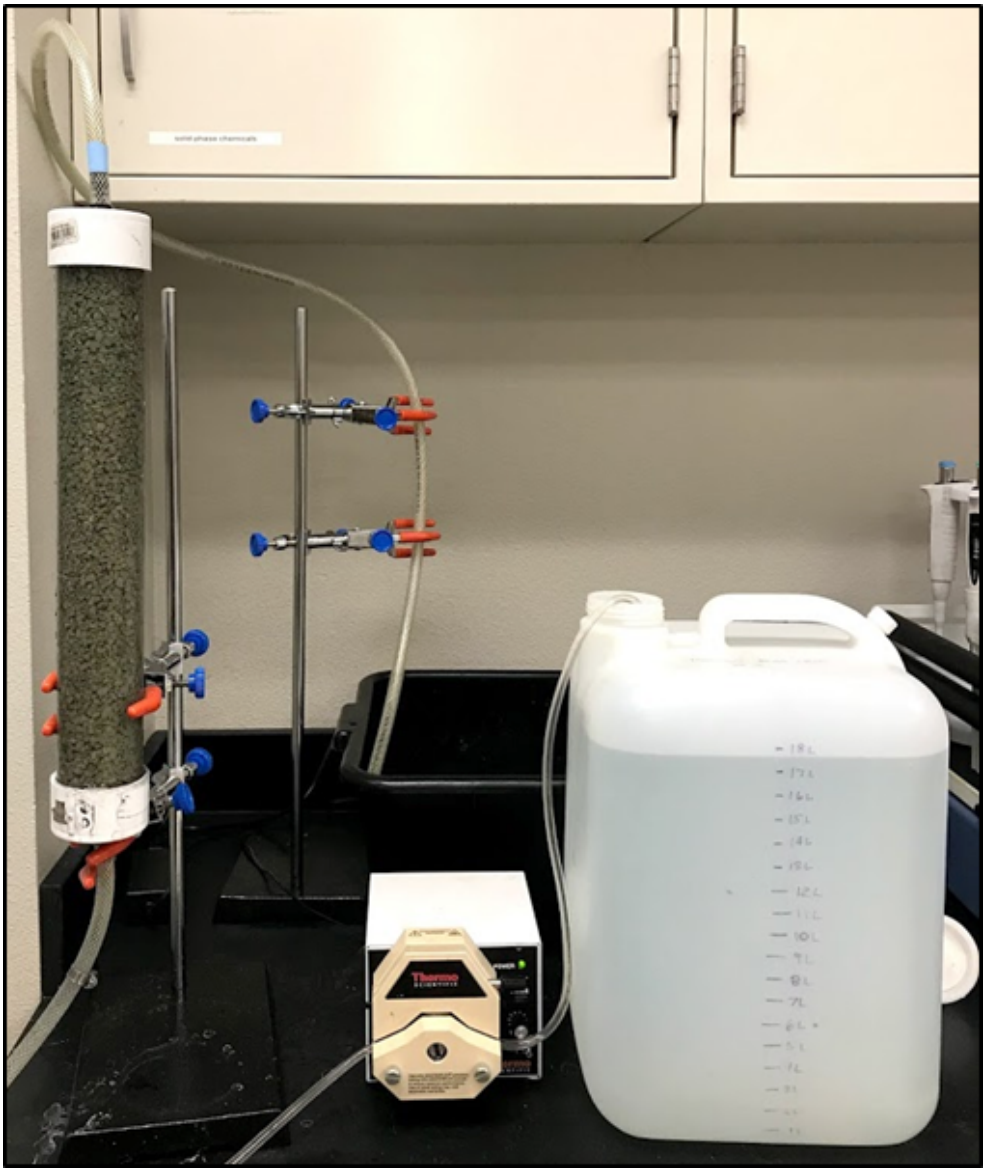

Figure 3.5. Example of large-scale column experiment.

3.2.8 Clinoptilolite surface analysis

Pre- and post-experiment clinoptilolite surface morphology and sorbed Fe distribution were analyzed using a scanning electron microscope (Zeiss SUPRA 35 SEM) equipped with energy dispersive x-ray spectroscopy (Noran System Six EDS). Samples were carbon-coated prior to analysis.

3.3 Results and discussion

3.3.1 Permeability comparison

Measured flow rates through Si fiber at packing densities of 0.073, 0.037, and 0.018 g/cm^3 were 0.06, 0.08, and 0.14 L/s, respectively. Results indicate that flow rate increased at lower packing

densities; however, dye tracers indicated preferential flow at packing densities of 0.037 and 0.018 g/cm^3. At all packing densities, Si fiber retained water in void spaces, restricting permeability. Si fiber at a packing density of 0.073 g/cm^3 resulted in an acceptable permeable arrangement without inducing bypass.

Clinoptilolite grains were slightly compacted after saturation, but permeability remained at 0.20 L/s for the duration of the experiments. This flow rate is nearly three times the flow rate allowed by Si fiber at 0.073 g/cm^3. Results indicate that clinoptilolite at a 4 × 8 mesh grain size has a greater permeability than Si fiber. Packing densities of 0.073 g/cm^3 for Si fiber and Si+APTES, and 0.73 g/cm^3 for clinoptilolite were selected for use in batch sorption calculations and column experiments.

3.3.2 Batch sorption comparison and adsorption isotherms

Specific sorption of Fe on the bare Si fiber did not increase with greater Fe concentration, but specific sorption of Fe with Si+APTES and clinoptilolite did increase with greater concentration of Fe (Fig. 3.6). Specific sorption of Fe^{2+} by Si fiber was minimal for all concentrations, therefore further experimentation with bare Si fiber was abandoned. Specific sorption of Fe^{2+} was greater for Si+APTES than clinoptilolite at all concentrations (Fig. 3.6). To evaluate specific sorption at possible packing densities, specific sorption values were multiplied by packing densities of 0.073 and 0.73 g/cm^3 for Si+APTES and clinoptilolite, respectively (Fig. 3.7). The packing density adjusted values of specific sorption indicate that a greater amount of Fe^{2+} would be sorbed per container volume (mg/cm^3) for clinoptilolite than Si+APTES (Fig. 3.7).

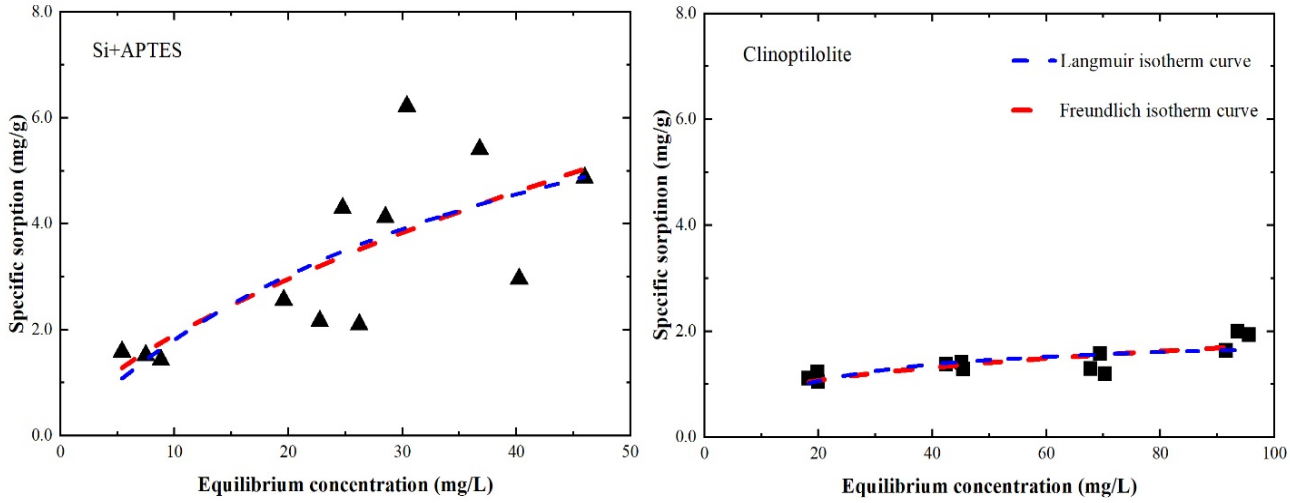

Figure 3.6: Adsorption equilibria of Fe^{2+} on Si+APTES and clinoptilolite at pH of 3.0 with associated Langmuir and Freundlich isotherm curves for equivalent surface areas.

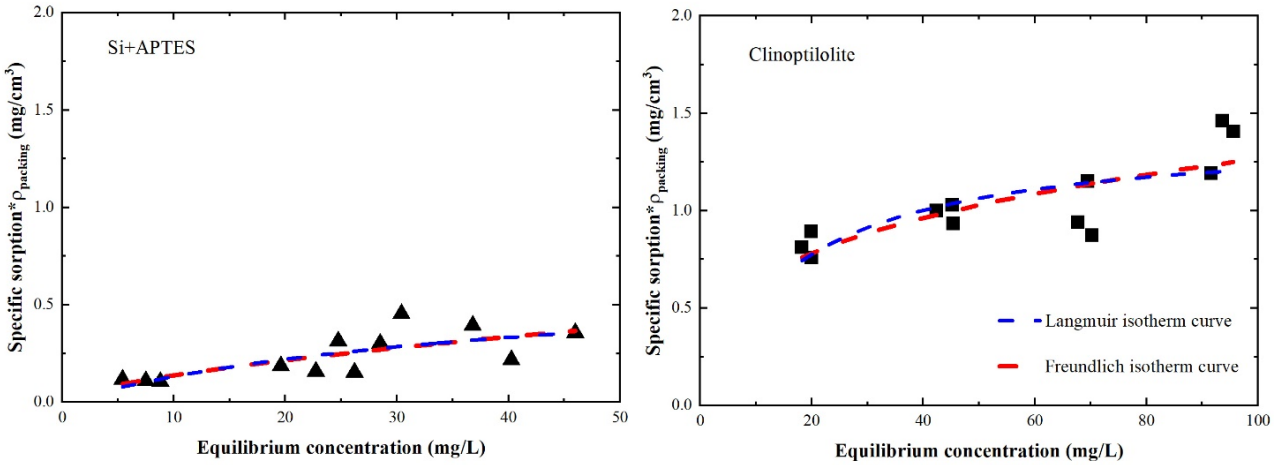

Figure 3.7: Packing-density normalized, adsorption equilibria of Fe^{2+} on Si+APTES and clinoptilolite at pH of 3.0 with associated Langmuir and Freundlich isotherm curves.

Neither the Langmuir or Freundlich isotherms were representative of the specific sorption results for Si+APTES or clinoptilolite. R^2 values calculated for the Langmuir isotherm were 0.545 and 0.544 for Si+APTES and clinoptilolite, respectively (Table 3.1). The chelating functional group of Si+APTES and the microporous structure of clinoptilolite do not provide homogeneous surfaces, and sorption likely is not occurring in a monolayer as predicted by the Langmuir model.

R^2 values calculated for the Freundlich isotherm were 0.541 and 0.632 for Si+APTES and clinoptilolite, respectively (Table 3.1). This model does not well represent the metal capture by Si+APTES likely because Fe removal is occurring by chelation (multi-parameter binding event) rather than adsorption (one-to-one binding event). The Freundlich isotherm model is a better fit for clinoptilolite because the model assumes a heterogeneous surface where multilayer sorption can occur.

Table 3.1: Parameter estimates for Langmuir and Freundlich isotherm models for experimental results of Fe^{2+} adsorption on Si+APTES and clinoptilolite at pH of 3.0.

[K_L= Langmuir constant related to free energy of adsorption; q_{max} = maximum monolayer adsorption; R^2 = coefficient of determination; K_f = Freundlich constant related to maximum adsorption; n = constant related to sorption intensity]

Model type	Si+APTES	Clinoptilolite
Langmuir isotherm		
K_L (L/mg)	0.024 ± 0.028	0.061 ± 0.027
q_{max} (mg/g)	9.225 ± 6.164	1.936 ± 0.214
R^2	0.545	0.544
Freundlich isotherm		
K_f (mg/g)	0.436 ± 0.356	0.436 ± 0.135
n	1.564 ± 0.590	3.337 ± 0.849
R^2	0.541	0.632

The orange surfaces of Si+APTES and clinoptilolite following batch sorption experiments indicate that Fe-(oxyhydr)oxides are formed as a result of capture and interaction with the substrate surfaces (Fig. 3.8).

Figure 3.8: (Left to right) 12 g of bare silica felt, 12 g of Si+APTES, and 5.4 g of clinoptilolite before (top row) and after (bottom row) batch sorption experiments. Orange color is due to sorbed/precipitated Fe-(oxyhydr)oxides.

3.3.3 Column experiments

Small-scale column experiments with 150 g of clinoptilolite (6,000 m^2 surface area), 15 g of Si + APTES (270 m^2 surface area), and 1,000 mg/L acidic Fe solutions indicate greater total Fe removal by clinoptilolite, with exhaustion occurring at approximately 60 minutes for Si+APTES and 360 minutes for clinoptilolite (Fig. 3.9). Values for total Fe removal (R_{total}) were normalized by substrate mass and surface area, indicating equivalent Fe removal per g (R_M; mg/g) for the two substrates, and a greater Fe removal per m^2 of surface area (R_{SA}) for Si+APTES (Table 3.2). For both substrates, Fe-(oxyhydr)oxide precipitation occurred because of buffering processes, resulting in effluent pH increasing from 3.0 to 6.3 for Si+APTES and 3.0 to 5.9 for clinoptilolite

(Fig. 3.10). As small-scale column experiments continued, effluent pH gradually decreased to 3.0 for Si+APTES and 3.4 for clinoptilolite after 360 minutes (Fig. 3.10).

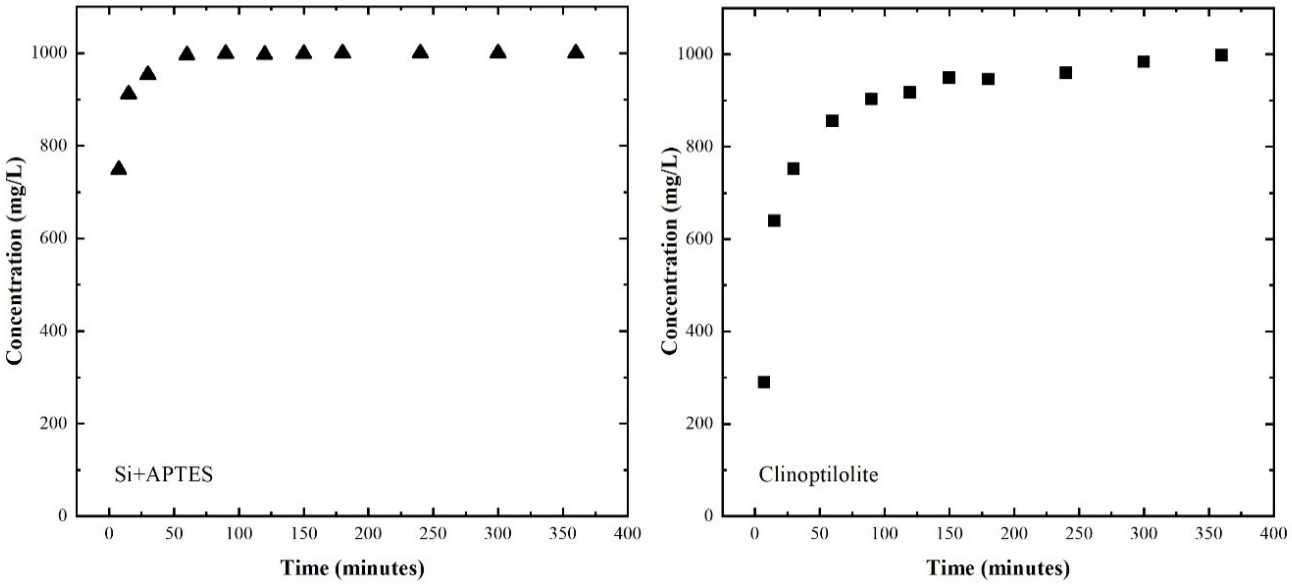

Figure 3.9: Sorption of Fe^{2+} to Si+APTES (left) and clinoptilolite (right) in small-scale column experiments.

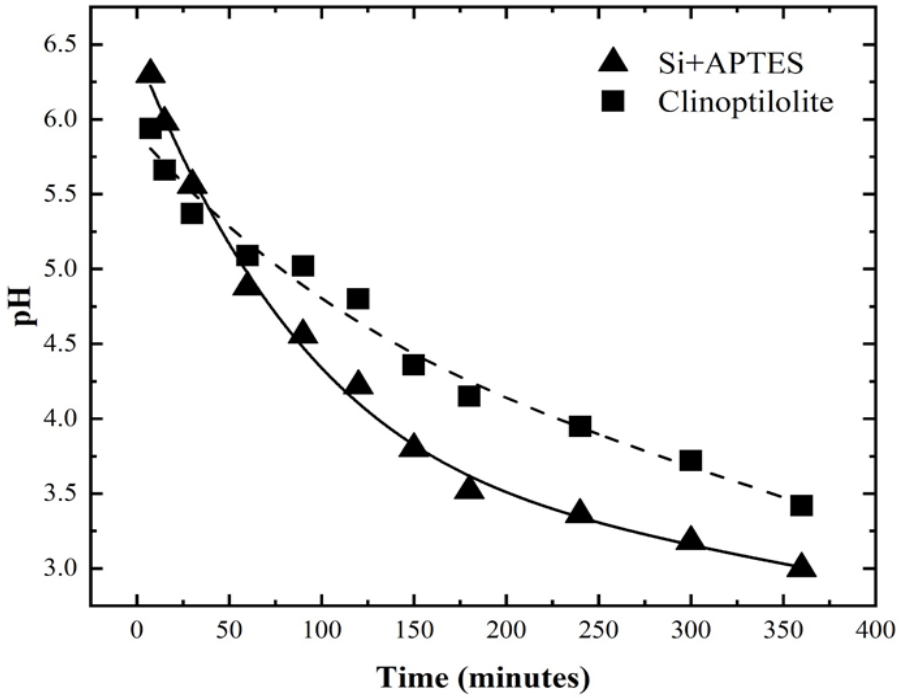

Figure 3.10: pH change during a small-scale column experiment at 20 ºC. Initial pH of solution was 3.0, and amount of substrate for clinoptilolite and Si+APTES was 150 g and 15 g, respectively.

Given greater total Fe removal for clinoptilolite in small-scale column experiments, large-scale column experiments were instituted to evaluate potential changes in Fe removal with an increase

in scale. Results indicate that quadrupling the amount of clinoptilolite in the columns increased time to exhaustion by nearly a factor of 17 (Fig. 3.11). Normalized R_{total} values reveal that the additional clinoptilolite increased Fe removal per g by nearly 50 mg/g and Fe removal per m^2 of surface area by 1.5 mg/m^2 (Table 3.2). Initial column effluent showed an increase in pH from 3.0 to 7.0, resulting in Fe-(oxyhydr)oxide precipitation, followed by a gradual decrease of pH to 3.7 by the end of the experiment (Fig. 3.11).

Table 3.2: Results from large- and small-scale column experiments.

[SA = surface area; R_{total} = total mg of Fe removed; R_M = Fe removed per g of substrate (mg/g); R_{SA} = Fe removed per m^2 of substrate surface area]

Substrate	Mass (g)	SA (m^2)	R_{total} (mg)	R_M (mg/g)	R_{SA} (mg/m^2)
Small-scale column					
Si+APTES	15	270	137	9.1	0.5
Clinoptilolite	150	6,000	1,364	9.1	0.2
Large-scale column					
Clinoptilolite	600	24,000	40,302	67.2	1.7

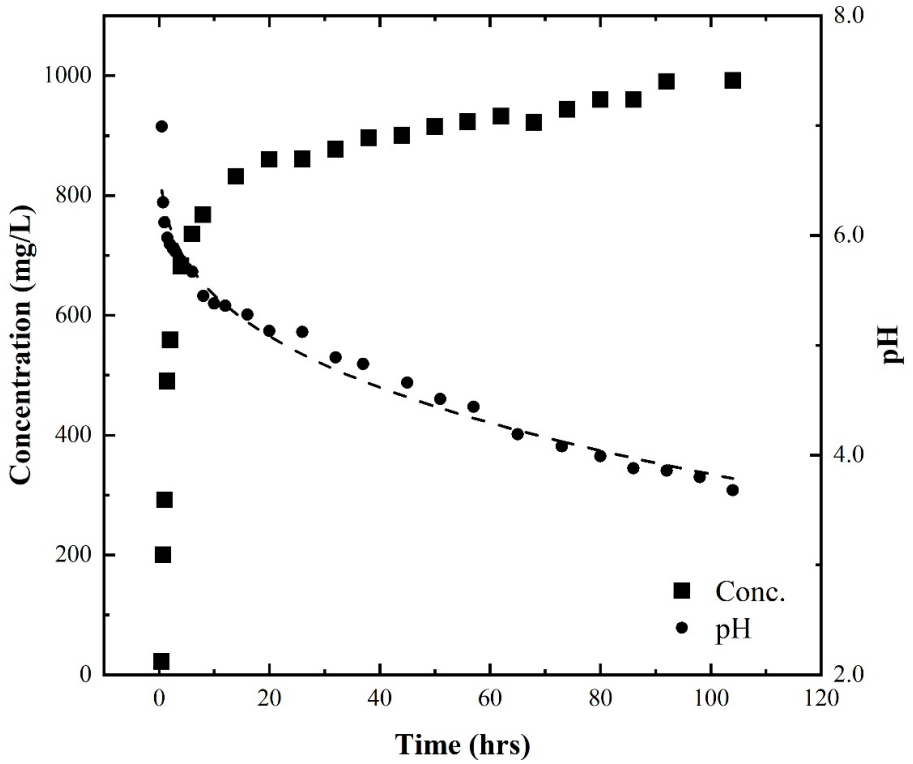

Figure 3.11: Sorption of Fe^{2+} to clinoptilolite and pH change during large-scale column experiments—average results of triplicate experiments. Initial pH of Fe solution was 3.0 ± 0.1.

In both small and large-scale column experiments, Fe removal was initially high followed by a decreasing rate until the end of the experiment. The largest removal of Fe from solution during the early period of the small- and large-scale column experiments likely is a result of the corresponding change in pH, which decreased Fe solubility and resulted in precipitation of Fe (oxyhydr)oxides (Hem & Cropper, 1959). The subsequent period of a gradual increase in Fe

concentration in solution and decreasing pH likely is a reflection of decreasing sorption site availability as the surface and pores become saturated with sorbed Fe (Hashemian et al., 2013). Greater Fe removal in large-scale column experiments can be attributed to the greater amount of clinoptilolite and potential surface interaction over the given flowpath in the column.

3.3.4 SEM Analysis

The irregular surface topography visible in Figure 3.12 and micropores present throughout clinoptilolite grains (not visible in the figure due to their likely <1 nm pore diameter) result in a large surface area available for sorption of ions (Pandová et al., 2018). The post-experiment spectral map of Fe on the clinoptilolite surface indicates a diffuse capture of Fe across the grain. There are no obvious patterns that indicate greater capture on any surface area or large accumulations suggestive of substantial mineral precipitation locations.

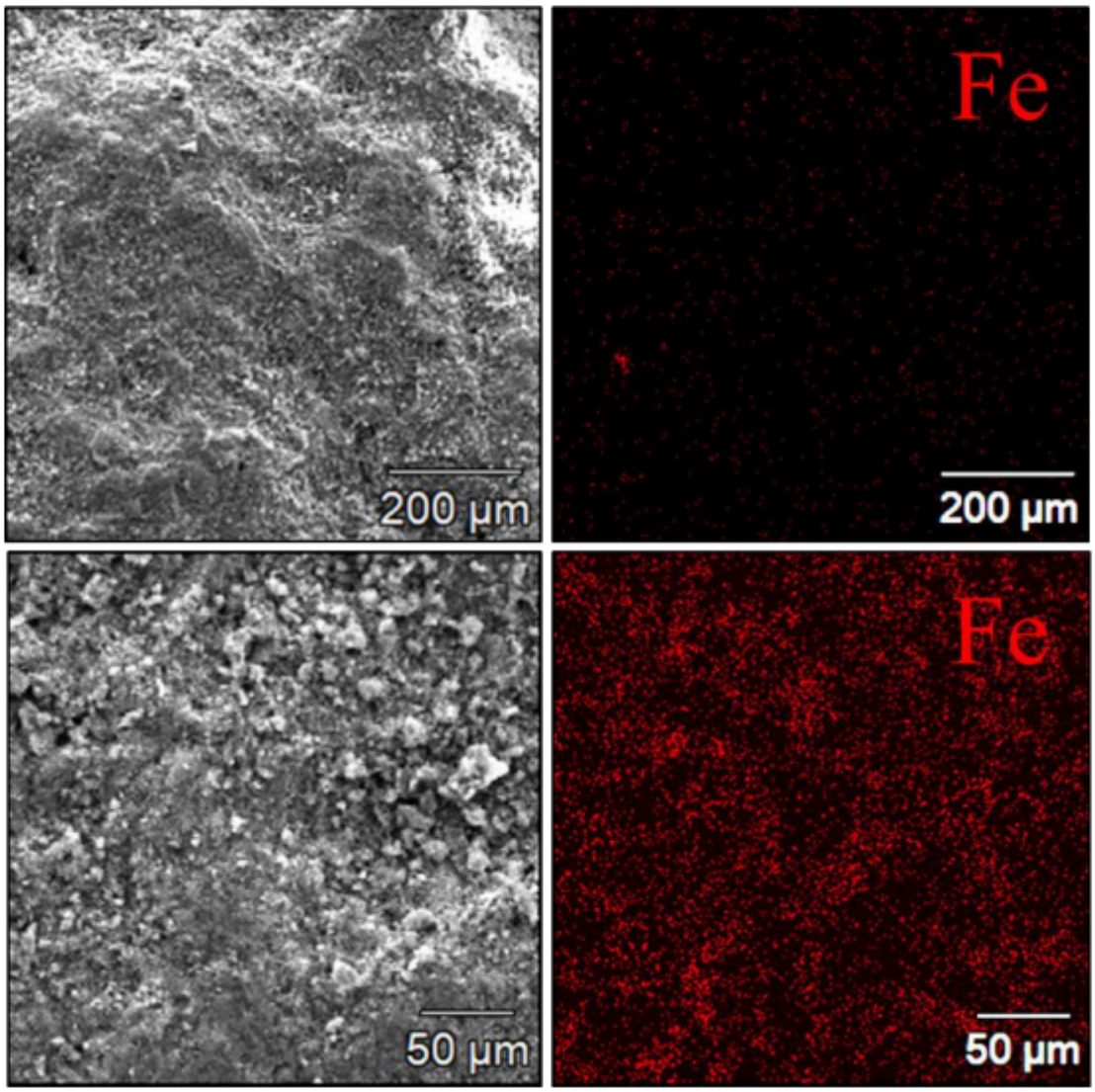

Figure 3.12: Images of pre- (upper) and post-experiment (lower) clinoptilolite surface at 380X magnification (left) with corresponding spectral map of Fe (right), where Kα peak was used for element identification.

3.3.5 Substrate selection

Si+APTES demonstrated high specific sorption of Fe in batch sorption experiments and has potential application in lower flow, passive treatment systems. The greater permeability, large surface area, and ion-exchange properties of clinoptilolite make these natural zeolite grains a better choice as a reactive substrate for passive treatment of acidic drainage, particularly at higher flows. Clinoptilolite has variable sized pores, including angstrom-scale pores, which can increase diffusion times and result in a continuum of sorption events that enhances their metal removal capability. Additionally, the readily available clinoptilolite requires minimal surface preparation and can be easily incorporated into passive treatment systems such as this study's modular treatment system.

CHAPTER 4

DEPLOYMENT OF PROTOTYPE

4.1 Introduction

The Great Falls Coal Field near Great Falls, Montana, was a heavily mined region in the late 1800s to mid-1900s (Rossillon, McCormick, & Hufstetler, 2009). To this day, ARD seeps from abandoned mine portals, adits, and coal seams, polluting streams and scarring hillsides. Several sites experiencing ARD in the Great Falls Coal Field were scouted as potential sites for a field deployment of the modular treatment system prototype. Discharge at a location near Cottonwood Mine No. 6 (CW-2) was selected as a treatment site based on documented flow rate, pH, and dissolved Fe concentration considered suitable for a prototype of the modular treatment system containing clinoptilolite as the reactive substrate.

Figure 4.1: Acid rock drainage flowing from an abandoned coal mine near Great Falls, Montana.

Historical minimum, average, and 75th percentile flow rates at CW-2 were 30, 68, and 79 L/min (Hydrometrics, Inc. & TKT Consulting, LLC, 2012). Historical minimum, average, and maximum pH values were 2.6, 2.9, and 3.1 (Hydrometrics, Inc. & TKT Consulting, LLC, 2012). Historical minimum, average, and maximum dissolved Fe concentrations were 646, 756, and 840 mg/L (Hydrometrics, Inc. & TKT Consulting, LLC, 2012). Conditions for installation of the treatment system included stream banks composed primarily of mud with some small rocks. Field deployment of the modular treatment system at site CW-2 occurred from June 16–21, 2019. The goal of the deployment was to monitor hydraulic performance and Fe removal of the modular treatment system under field ARD conditions for 3–5 days.

4.2 Methods

4.2.1 Construction

Initial construction of the 6-cartridge configuration occurred over three days (June 16–18, 2019). A hole approximately 2.7 m (L) × 1.2 m (W) × 1.4 m (H) was excavated with shovels and picks beside a Parshall flume previously installed near the ARD source at site CW-2 (Fig. 4.2). An additional 0.2 m was excavated from the bottom of the hole for every 0.6 m in downgradient length to accommodate the necessary hydraulic gradient for the modular treatment system (Fig. 4.3). Lastly, a 3-m long drain was excavated to prevent water from filling the excavated hole (Fig. 4.3).

Figure 4.2: Hole and drain excavated for the modular treatment system next to ARD channel.

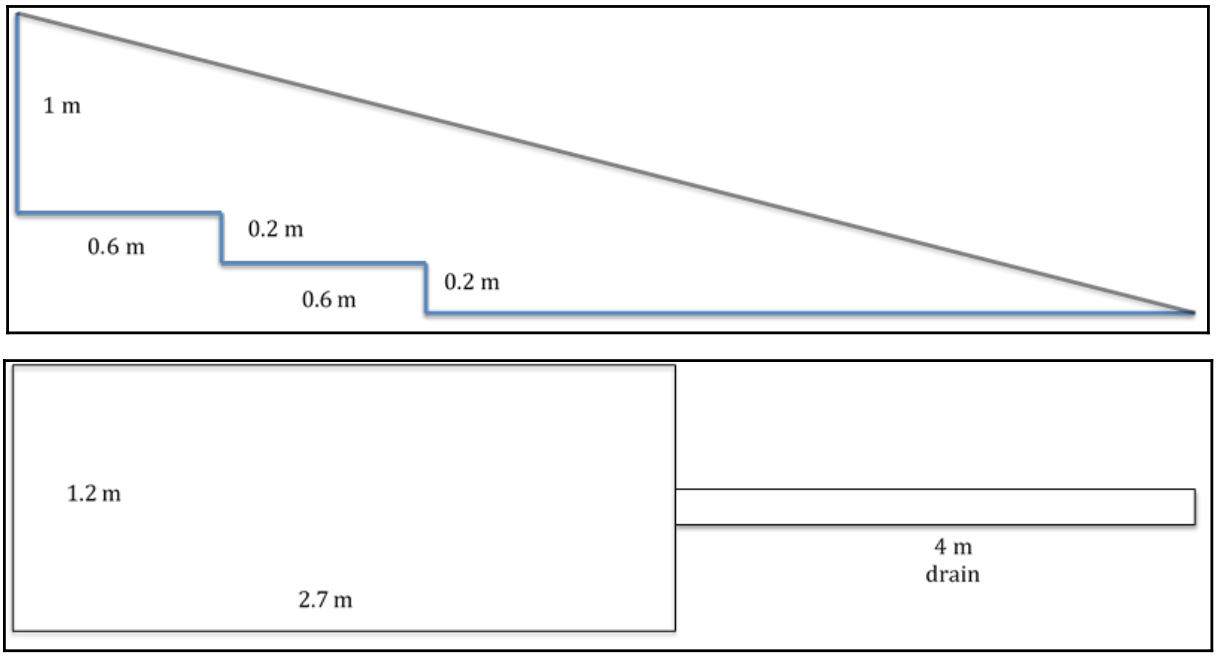

Figure 4.3: Profile (top) and map (bottom) view of excavation plan for the modular treatment system.

Once excavation was complete, the modular treatment system's outer framework was assembled and clinoptilolite-filled cartridges were installed (Figs. 4.4–4.9). Following system assembly, the entry-weir was connected briefly (Fig. 4.10) but was replaced with a polyethylene gutter drain due to leakage occurring between the entry-weir and entry elbow (Fig. 4.11). A dam was constructed at the ARD source from local sediments and rocks to create a hydraulic head pool sufficient to route ARD through the gutter drain and into the treatment system (Fig. 4.12).

Figure 4.4: First cartridge installation to the modular treatment system.

Figure 4.5: Second cartridge installation to the modular treatment system.

Figure 4.6: Third cartridge installation to the modular treatment system.

Figure 4.7: Fourth cartridge installation to the modular treatment system.

Figure 4.8: Fifth cartridge installation to the modular treatment system.

Figure 4.9: Sixth cartridge installation to the modular treatment system.

Figure 4.10: Entry-weir connected to the modular treatment system.

Figure 4.11: Entry-weir replaced with gutter drain due to leakage.

Figure 4.12: Damn constructed at ARD source to route ARD into gutter drain.

Following the initial setup period, ARD began flowing through the 6-cartridge configuration on June 19th at 0930, and discharge and water chemistry were monitored for 24 hrs. Fe removal was minimal during this time, so cartridges were refreshed with clinoptilolite and a 2-cartridge configuration was tested for an additional 24 hrs, beginning at 1230 on June 20th.

4.2.2 Flow rate measurements

Flow rates were measured with a 5-L bucket and a stopwatch for the seep, as well as for influent and effluent flow rates during field experiments. Initial ARD flow rate were measured from the Parshall flume present near the source of the seep discharge. Influent flow rates were measured from the gutter drain and effluent flow rates were measured from the final PVC elbow that directed ARD back into the drainage channel.

4.2.3 Water chemistry measurements

Polypropylene twist valves had been installed in the outer framework between the units of the modular treatment system (indicated by numbers 2–6 in Fig. 4.13 and #2 is visible in Fig. 4.11) to allow for collection of water samples before and after each cartridge. Dissolved oxygen (DO), pH, temperature, conductivity, and oxidation-reduction potential (ORP) were measured with a HANNA HI-9829 multi-parameter field probe at sampling locations 1, 4, and 7 for the 6-cartridge configuration and locations 1, 2, and 3 for the 2-cartridge configuration. Fe concentration was measured with a Hach DR3900 spectrophotometer at locations 1–7 for the 6-cartridge configuration and locations 1–3 for the 2-cartridge configuration.

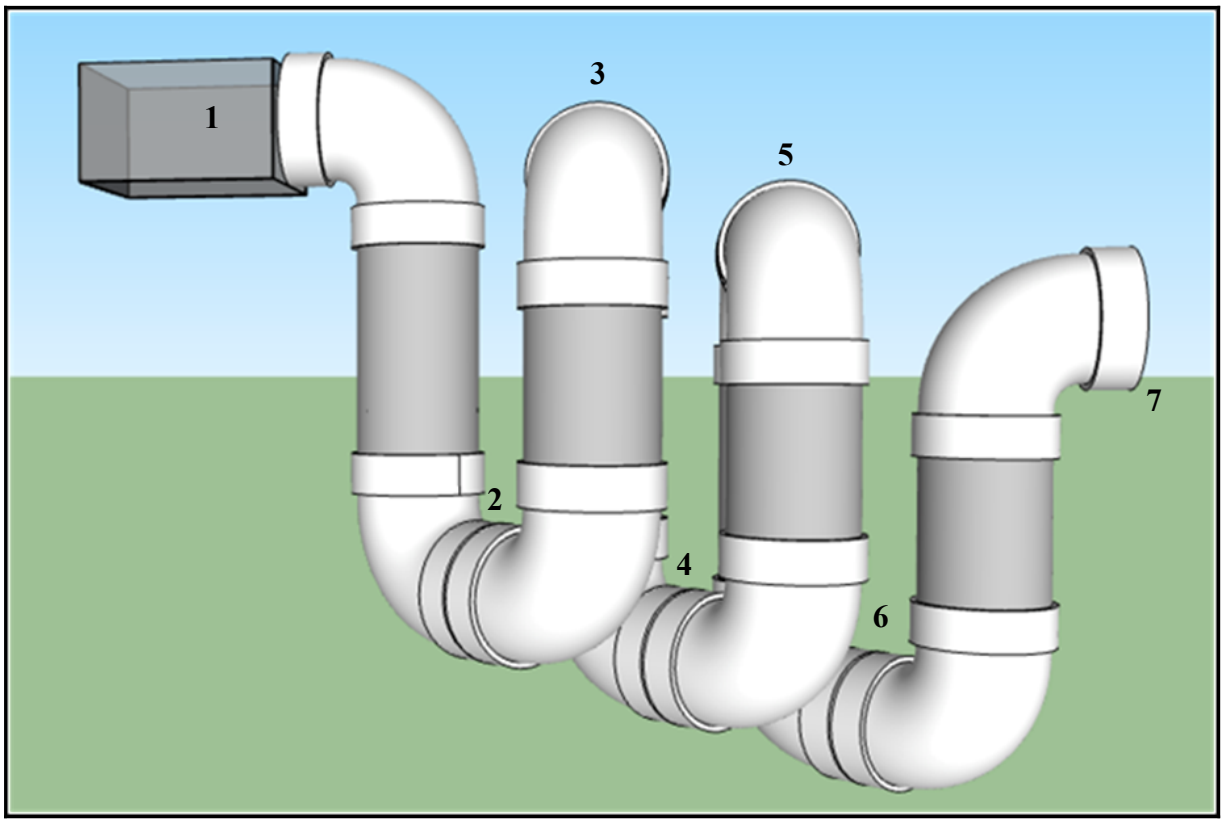

Figure 4.13: Valve and water sampling locations for the modular treatment system.

For the 6-cartridge configuration, water samples were collected and analyzed for Fe at 0, 2.5, 4.5, 6.5, 8.5, 10.5, and 24 hr after the start of treatment. For the 2-cartridge configuration, water samples were collected and analyzed for Fe at 0, 0.5, 2.5, 4.5, 6.5, 8.5, and 24 hr after the start of treatment. Quality control and accuracy were checked with instrument blanks, replicate samples, calibration standards, and matrix spikes over the course of the study. No false positives were reported. A 2% error was determined for all measured Fe concentrations.

4.3 Results and discussion

4.3.1 Flow rate measurements

The initial ARD flow rate at the CW-2 site was measured at approximately 30 L/min on June 19th. This flow rate is equivalent to the historical low previously measured at the site (Hydrometrics & TKT Consulting, 2012). During the startup period of the 6-cartridge configuration field test, it was determined that treatment system could not permit this flow rate due to a lack of hydraulic head. For this reason, influent ARD routed into the system was reduced to 4 L/min. A flow rate of 4 L/min was sustained for both 6- and 2-cartridge configurations. It is hypothesized that a lack of hydraulic head rather than a lack of permeability is responsible for the low flow rate through the treatment system. Re-configuring the entry so that the gutter drain and entry-elbow are connected and sealed could increase hydraulic head.

4.3.2 Water chemistry measurements

Initial ARD conditions during the 6-cartridge configuration field deployment ranged from 2.49 to 2.60 pH with initial Fe concentrations ranging from 552 to 586 mg/L. Monitoring results indicate little to no change in pH between sampling locations 1 and 4 and only a slight increase in effluent pH during the first 4.5 hours (0930–1400) (Table 4.1). Fe removal was also minimal during the 24 hours of monitoring (Table 4.1).

Table 4.1: Water chemistry results from 6-cartridge configuration of the modular treatment system during 24-hr field deployment.
[LOC. = sampling location at designated unit (1, 2, 3, etc.); Fe = total dissolved iron (mg/L)]

DATE	TIME	VARIABLE	LOC.1	LOC.2	LOC.3	LOC.4	LOC.5	LOC.6	LOC.7
6/19/19	0930	pH	2.58			2.63			2.88
6/19/19	0930	Fe (mg/L)	562	573	576	546	570	558	557
6/19/19	1200	pH	2.55			2.57			2.69
6/19/19	1200	Fe (mg/L)	575	575	573	574	567	579	573
6/19/19	1400	pH	2.60			2.57			2.66
6/19/19	1400	Fe (mg/L)	552	554	551	557	547	553	544
6/19/19	1600	pH	2.61			2.59			2.65
6/19/19	1600	Fe (mg/L)	586	575	551	580	565	573	577
6/19/19	1800	pH	2.58			2.57			2.61
6/19/19	1800	Fe (mg/L)	562	560	568	563	570	558	552
6/19/19	2000	pH	2.59			2.63			2.65
6/19/19	2000	Fe (mg/L)	565	567	572	572	572	563	567
6/20/19	0930	pH	2.49			2.50			2.52
6/20/19	0930	Fe (mg/L)	565	577	563	558	571	550	576

Initial ARD conditions during the 2-cartridge configuration field deployment ranged from 2.49 to 2.60 pH with initial Fe concentrations ranging from 559 to 581 mg/L. Monitoring results indicate a marginal increase in pH during the first 4.5 hr with no effect on pH following this period (Table 4.2). The first effluent to exit the system removed approximately 73 mg/L of Fe; however, Fe removal was negligible for the remainder of the deployment (Table 4.2).

Table 4.2: Water chemistry results from 2-cartridge configuration of the modular treatment system during 24-hr field deployment.
[LOC. = sampling location at designated unit (1, 2, 3, etc.); Fe = total dissolved iron (mg/L)]

DATE	TIME	VARIABLE	LOC.1	LOC.2	LOC.3
6/20/19	1230	pH	2.59	2.61	2.74
6/20/19	1230	Fe (mg/L)	562	561	489
6/20/19	1300	pH	2.59	2.61	2.74
6/20/19	1300	Fe (mg/L)	571	572	570
6/20/19	1500	pH	2.62	2.64	2.66
6/20/19	1500	Fe (mg/L)	581	579	582
6/20/19	1700	pH	2.51	2.56	2.59
6/20/19	1700	Fe (mg/L)	567	559	569
6/20/19	1900	pH	2.55	2.55	2.55
6/20/19	1900	Fe (mg/L)	571	571	573
6/20/19	2100	pH	2.55	2.55	2.55
6/20/19	2100	Fe (mg/L)	574	580	580
6/21/19	1230	pH	2.49	2.49	2.48
6/21/19	1230	Fe (mg/L)	559	560	560

The difference in laboratory and field results, in terms of Fe removal by clinoptilolite, likely was a result of pH differences and protonation of the mineral surface. Laboratory experiments were conducted at a pH of 3.0 while field pH varied from 2.49-2.60 during deployment. The following chapter investigates the effect of pH and competing cations on the sorption of Fe to clinoptilolite and the desorption of Fe from clinoptilolite.

CHAPTER 5

PROTONATION AND DESORPTION EXPERIMENTS

5.1 Introduction

Results from the June field deployment of the modular treatment system near Stockett, Montana, were vastly different than bench-scale experiments—Fe^{2+} sorption by clinoptilolite was minimal. It was hypothesized that the unexpectedly acidic field conditions (pH of 2.5) resulted in the protonation of clinoptilolite surfaces, which neutralized the residual negative surface charge that allows sorption to occur (Nelson et al., 2019; Parks, 1967). In addition to protons, other dissolved metals present in ARD compete for sorption sites, decreasing sorption of other metals or replacing previously sorbed metals (Aston et al., 2010). The replacement or release of previously sorbed metals is often referred to as desorption (Aston et al., 2010; Limousin et al., 2007).

For this investigation, batch sorption/protonation experiments were conducted with Si, Si+APTES, and clinoptilolite across a range of acidic pH values to observe the effects of pH on sorption/desorption of Fe^{2+}. Additionally, batch desorption experiments were conducted by suspending Fe-saturated clinoptilolite in a variety of waters at various pH values and temperatures. The goal of this portion of the investigation was to determine the reason for the lack of Fe removal in the treatment system during the field deployment and examine the retention of sorbed Fe on clinoptilolite under possible variations in environmental conditions.

5.2 Materials and Methods

The same Si, Si+APTES, and clinoptilolite were used for the protonation and desorption experiments.

5.2.1 Protonation experiments

12 g of Si, 12 g of Si+APTES, and 5.4 g of clinoptilolite (equivalent surface areas of 216 m^2) were placed in polyester strainers and suspended in Fe-rich solutions (100 mg/L) at various pH values (2.5, 2.6, 2.7, 2.8, 2.9, 3.0, 3.25, 3.50, 3.75, 4.0). Fe-rich solutions were created by dissolving an appropriate mass of ferrous-sulfate heptahydrate [$FeSO_4 \cdot 7H_2O$] in ultrapure water. Solution pH was maintained through addition of H_2SO_4. Solutions were mixed on a shaker table for 6 hr at 100 rpm, and equilibrium Fe concentration was measured with FerroVer total iron reagent and a spectrophotometer after 6 hr.

5.2.2 Desorption experiments

Desorption experiments were conducted by suspending 5.4 g of clinoptilolite in polyester strainers within various solutions for 6 hr on a shaker table at 100 rpm. Three water types (ultrapure, natural stream, and Ni-rich) were used to create 12 solution types. Natural stream water was collected from Paradise Creek, Moscow, Idaho, and a Ni-rich solutions was created by dissolving 112 mg of Ni(II) sulfate hexahydrate ($H_{12}NiO_{10}S$) in ultrapure water for a Ni(II)

concentration of 25 mg/L. A walk-in freezer and H_2SO_4 were utilized to adjust temperature and pH and generate the following solution types of each of the ultrapure, natural stream, Ni-rich water types: neutral pH at 5 ºC, neutral pH at 20 ºC, pH 2.0 at 20 ºC, and pH 4.0 at 20 ºC. Aqueous Fe concentration was measured with FerroVer total iron reagent and a spectrophotometer every hr. Experiments were conducted in triplicate.

5.3 Results and discussion

5.3.1 Protonation experiments

Fe removal by bare Si fiber was negligible at all pH values; therefore, graphical results are not included. Fe sorption with Si+APTES was minor for pH 2.5 to 2.9 but did increase at a low rate (Fig. 5.1). At pH 3.0, specific sorption increased from 0.8 mg/g to 4.3 mg/g. From pH 3.0 to 4.0, specific sorption results were variable but remained greater than 2.5 mg/g. Results indicate that Si+APTES may be applicable as a sorptive substrate in mildly acidic ARD (pH ≥ 3.0).

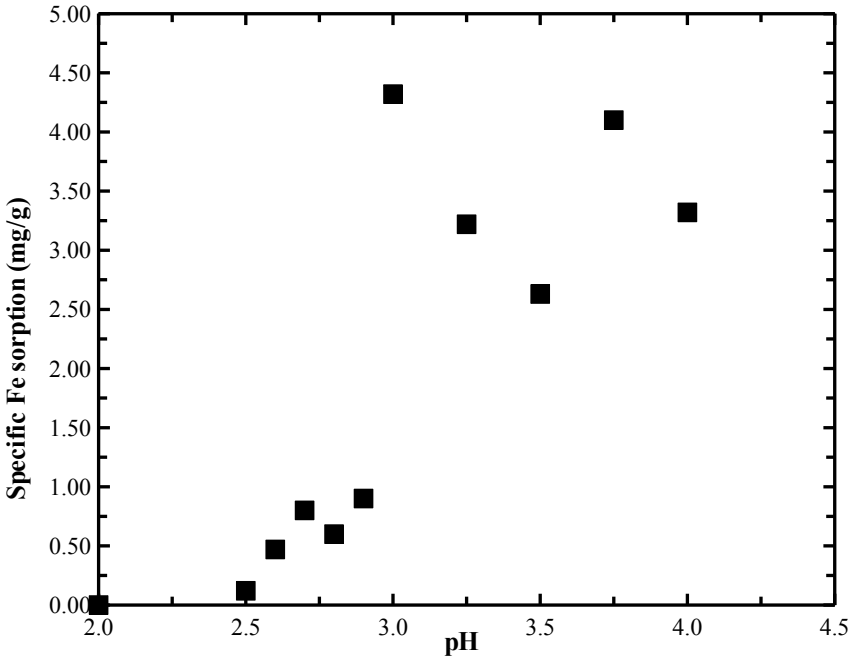

Figure 5.1: Fe sorption on Si+APTES at various pH values in protonation experiments.

At pH 2.5, Fe specific sorption on clinoptilolite was 0.0 mg/g (Fig. 5.2). Specific sorption increased gradually as pH increased until pH 3.5, where specific sorption nearly doubled from 1.7 mg/g to 3.1 mg/g. Specific sorption at pH 4.0 was 3.5 mg/g. These results confirm the hypothesis that the low field pH resulted in protonation of the zeolite surfaces and the poor performance of the modular treatment system. Results indicate that clinoptilolite may be applicable as a sorptive substrate in mildly acidic ARD (pH ≥ 3.0).

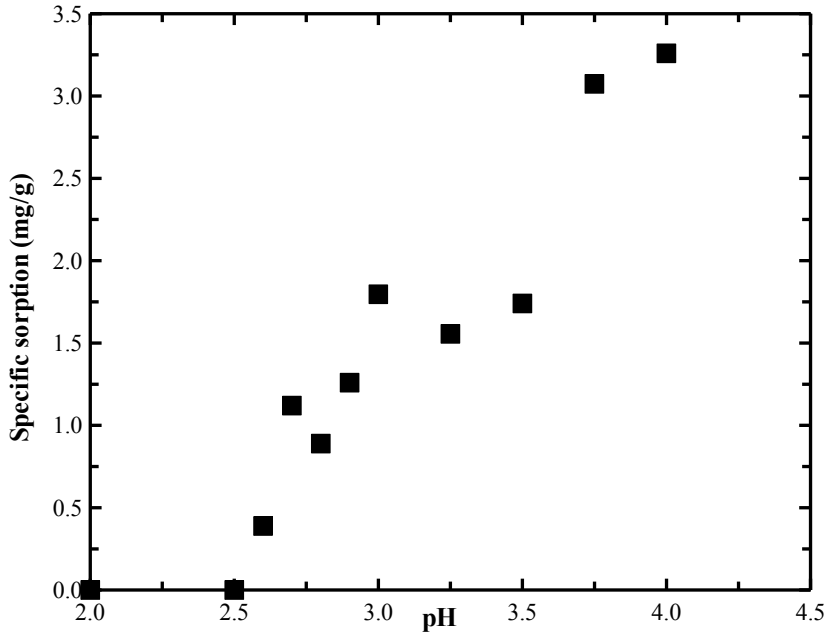

Figure 5.2: Fe sorption on clinoptilolite at various pH values in protonation experiments.

5.3.2 Desorption experiments

Results from desorption experiments with ultrapure water indicate that clinoptilolite retained sorbed Fe at 5 ºC and 20 ºC under neutral and mildly acidic (pH 4.0) conditions (Fig. 5.3). Competing protons (surface protonation) in the pH 2.0 solution had the greatest effect on desorption—removing 2.8 mg of Fe over 6 hr (Fig. 5.3).

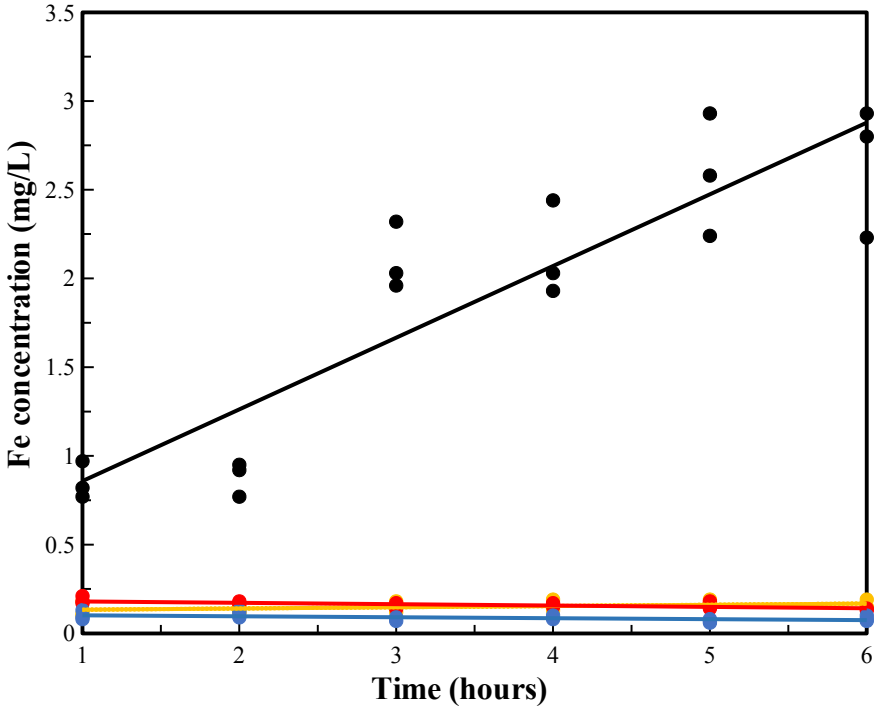

Figure 5.3: Desorption of Fe from clinoptilolite in ultrapure water over time at 5 ºC (blue), 20 ºC (red), pH of 2 (black), and pH of 4 (yellow).

Results from desorption experiments with natural stream water indicate that Fe desorption was greater in natural stream water than ultrapure and Ni-rich waters at all temperatures and pH values (Fig. 5.4). The pH 2.0 solution removed 7.9 mg of Fe over 6 hr (Fig. 5.4).

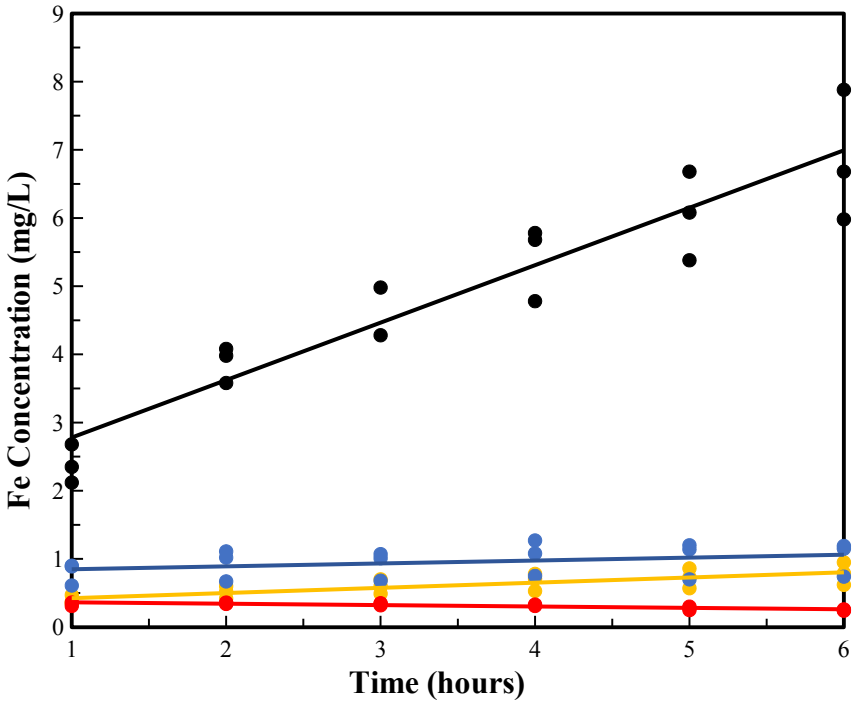

Figure 5.4: Desorption of Fe from clinoptilolite in natural stream water over time at 5 ºC (blue), 20 ºC (red), pH of 2 (black), and pH of 4 (yellow).

Results from desorption experiments in Ni-rich water indicate that the competing divalent ion had little effect on sorbed Fe at 5 ºC, 20 ºC, and mildly acidic (pH 4.0) conditions (Fig. 5.5). Results from the pH 2.0 experiment indicate that proton competition had the greatest effect on Fe desorption (Fig. 5.5).

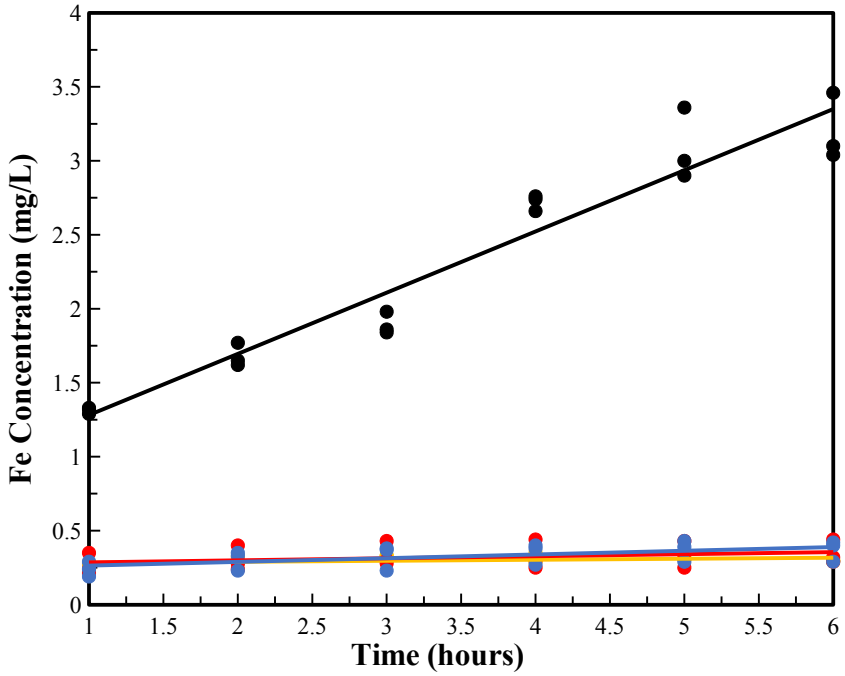

Figure 5.5: Desorption of Fe from clinoptilolite in Ni-rich water over time at 5 ºC (blue), 20 ºC (red), pH of 2 (black), and pH of 4 (yellow).

CHAPTER 6

PROJECT CONCLUSIONS

Integrating complimentary treatment systems for acid rock drainage (ARD) remediation can assist in reducing acid, metal, and sulfate concentrations, and variable discharge rates can be spatially integrated with modular systems in relatively small footprints. A modular and expandable treatment design with individual systems can provide additional flexibility to assist with remediation, particularly with an evolving mine drainage composition. Flexibility of design, particularly a modular design that allows for refreshing of a treatment material, can reduce the impact of seasonal flux of discharge and metal concentrations, increase treatment efficacy, extend overall system life, decrease costs, and minimize ARD environmental impacts.

An ARD passive treatment system was designed as a modular, flexible device intended to be deployed upstream of a primary treatment system(s). All materials selected for the treatment system are corrosion-resistant materials that can withstand the high acidity of ARD. The physical design consists of three components: an entry weir that directs drainage into the system, an outer framework composed of individual pipe/elbow units, and reactive material cartridges that are inserted into each unit of the outer framework. The cartridges can be filled with a choice of reactive material(s) and can be removed, refreshed with new reactive material, and reinstalled without removing the outer framework. The modular design of the system allows additional units to be added to the system for a desired residence/contact time. Additionally, individual units can be positioned at various angles so that the modular treatment system expands or contracts to fit a desired space. The system is designed to be partially buried next to the drainage where ARD is routed into the system, exits the final unit, and drains back into the channel. The partial burial of the system provides stability and allows top elbows to be removed for cartridge removal/insertion.

Various substrates (sorbing surface) and surface modifications (metal capture enhancement) were evaluated for creation of a reactive substrate for insertion into the modular treatment system. The goal was to provide options for possible substrates that could be readily purchased and modified with potential ease of insertion/removal into/from the system. The focus of the substrate evaluation was selection of low isoelectric point substrates that would capture Fe and other metals from solution through sorption. Substrates—including steel plates, tungsten wire, silica felt/wool, and a natural silicate mineral (zeolite)—and multiple surface modifications—including metal nanoparticles, silica nanoparticles, mesoporous silica nanoparticles, and multiple chelators—were evaluated for potential use in the modular treatment system. Experimental results indicate that a manufactured silicate material (silica (Si) fiber) with chelator (APTES-functionalized Si fiber (Si+APTES)) and a zeolite mineral (clinoptilolite) are viable reactive substrates for use in the modular treatment system to treat mildly acidic ($pH \geq 3.0$).

Si+APTES demonstrated high specific sorption of iron in batch sorption experiments and has potential application in lower flow, ARD passive treatment systems. The greater permeability,

large surface area, and ion-exchange properties of clinoptilolite make these natural zeolite grains a better choice as a reactive substrate for passive treatment of mildly acidic drainage, particularly at higher flows. Additionally, the readily available clinoptilolite requires minimal surface preparation and can be easily incorporated into passive treatment systems.

Field deployment of the modular treatment system prototype with clinoptilolite indicated an allowable flow rate of 4 L/min at minimal head without any obvious leaks or flow bypass. The limited flow rate was a result of a lack of hydraulic head at the entrance to the system rather than a lack of permeability. Iron removal by clinoptilolite was minimal in 6- and 2-cartridge configurations during field deployment due to high acidity (pH of 2.5) and protonation of the clinoptilolite surfaces that reduced their effectiveness for metal capture.

Protonation experiments reveal that iron sorption by Si+APTES and clinoptilolite is negligible at a pH of 2.5 but increases with higher pH. Both substrates have potential as reactive substrates for treating mildly acidic ARD with a pH $\geq$ 3.0. Desorption experiments show that temperature has little effect on desorption of iron from clinoptilolite. Highest desorption of iron from clinoptilolite occurred in solutions at a pH of 2.0, suggesting that proton competition has the largest effect on iron desorption. Results suggest that clinoptilolite used for metal sorption can remain effective with pH flux as long as pH does not substantially drop below 3.0.

REFERENCES

Acres, R. G., Ellis, A. V., Alvino, J., Lenahan, C. E., Khodakov, D. A., Metha, G. F., & Andersson, G. G. (2012). Molecular structure of 3-aminopropyltriethoxysilane layers formed on silanol-terminated silicon surfaces. *The Journal of Physical Chemistry C*, *116*(10), 6289–6297. https://doi.org/10.1021/jp212056s

Akcil, A., & Koldas, S. (2006). Acid mine drainage: Causes, treatment and case studies. *Journal of Cleaner Production*, *14*(12), 1139–1145. https://doi.org/10.1016/j.jclepro.2004.09.006

Aksu, Z., & Gönen, F. (2004). Biosorption of phenol by immobilized activated sludge in a continuous packed bed: Prediction of breakthrough curves. *Process Biochemistry*, *39*, 599–613. https://doi.org/10.1016/S0032-9592(03)00132-8

Alcolea, A., Vázquez, M., Caparrós, A., Ibarra, I., García, C., Linares, R., & Rodríguez, R. (2012). Heavy metal removal of intermittent acid mine drainage with an open limestone channel. *Minerals Engineering*, *26*, 86–98. https://doi.org/10.1016/j.mineng.2011.11.006

Aston, J. E., Apel, W. A., Lee, B. D., & Peyton, B. M. (2010). Effects of cell condition, pH, and temperature on lead, zinc, and copper sorption to Acidithiobacillus caldus strain BC13. *Journal of Hazardous Materials*, *184*(1), 34–41. https://doi.org/10.1016/j.jhazmat.2010.07.110

August, E. E., McKnight, D. M., Hrncir, D. C., & Garhart, K. S. (2002). Seasonal variability of metals transport through a wetland impacted by mine drainage in the Rocky Mountains. *Environmental Science & Technology*, *36*(17), 3779–3786. https://doi.org/10.1021/es015629w

Baker, B. J., & Banfield, J. F. (2003). Microbial communities in acid mine drainage. *FEMS Microbiology Ecology*, *44*(2), 139–152. https://doi.org/10.1016/S0168-6496(03)00028-X

Barquist, K. N. (2009). *Synthesis and Environmental Adsorption Applications of Functionalized Zeolites and Iron Oxide/Zeolite Composites* (PhD thesis). University of Iowa.

Bigham, J. M., & Nordstrom, D. K. (2000). Iron and aluminum hydroxysulfates from acid sulfate waters. *Reviews in Mineralogy and Geochemistry*, *40*, 351–403. https://doi.org/10.2138/rmg.2000.40.7

Brooks, P., McKnight, D., & Bencala, K. (2001). Annual maxima in Zn concentrations during spring snowmelt in streams impacted by mine drainage. *Environmental Geology*, *40*(11–12), 1447–1454. https://doi.org/10.1007/s002540100338

Burakov, A. E., Galunin, E. V., Burakova, I. V., Kucherova, A. E., Agarwal, S., Tkachev, A. G., & Gupta, V. K. (2018). Adsorption of heavy metals on conventional and nanostructured materials for wastewater treatment purposes: A review. *Ecotoxicology and Environmental Safety*, *148*, 702–712.

Costello, C. (2003). *Acid Mine Drainage: Innovative Treatment Technologies* (52 p.). US Environmental Protection Agency.

Cotton, A. (2008). Dissolution kinetics of clinoptilolite and heulandite in alkaline conditions. *Bioscience Horizons*, *1*(1), 38–43. https://doi.org/10.1093/biohorizons/hzn003

Davis, J. A., & Leckie, J. O. (1978). Surface ionization and complexation at the oxide/water interface—II. Surface properties of amorphous iron oxyhydroxide and adsorption of metal ions. *Journal of Colloid and Interface Science*, *67*(1), 90–107. https://doi.org/10.1016/0021-9797(78)90217-5

Dold, B. (2017). Acid rock drainage prediction: A critical review. *Journal of Geochemical Exploration*, *172*, 120–132. https://doi.org/10.1016/j.gexplo.2016.09.014

Dzombak, D. A., & Morel, F. M. M. (1990). *Surface Complexation Modeling: Hydrous Ferric Oxide*. John Wiley & Sons, Inc.

Egiebor, N. O., & Oni, B. (2007). Acid rock drainage formation and treatment: A review. *Asia-Pacific Journal of Chemical Engineering*, *2*(1), 47–62. https://doi.org/10.1002/apj.57

Erdem, E., Karapinar, N., & Donat, R. (2004). The removal of heavy metal cations by natural zeolites. *Journal of Colloid and Interface Science*, *280*(2), 309–314. https://doi.org/10.1016/j.jcis.2004.08.028

Faghihian, H., Ghannadi Marageh, M., & Kazemian, H. (1999). The use of clinoptilolite and its sodium form for removal of radioactive cesium, and strontium from nuclear wastewater and Pb^{2+}, Ni^{2+}, Cd^{2+}, Ba^{2+} from municipal wastewater. *Applied Radiation and Isotopes*, *50*(4), 655–660. https://doi.org/10.1016/S0969-8043(98)00134-1

Fan, C., & Zhang, Y. (2018). Adsorption isotherms, kinetics and thermodynamics of nitrate and phosphate in binary systems on a novel adsorbent derived from corn stalks. *Journal of Geochemical Exploration*, *188*, 95–100. https://doi.org/10.1016/j.gexplo.2018.01.020

Gainer, G. M. (1993). *Boron Adsorption on Hematite and Clinoptilolite* [Technical Report, LA-SUB—94-64]. US Department of Energy, Los Alamos National Laboratory.

Gibert, O., Cortina, J. L., de Pablo, J., & Ayora, C. (2013). Performance of a field-scale permeable reactive barrier based on organic substrate and zero-valent iron for in situ remediation of acid mine drainage. *Environmental Science and Pollution Research*, *20*(11), 7854–7862. https://doi.org/10.1007/s11356-013-1507-2

Gibert, O., de Pablo, J., Luis Cortina, J., & Ayora, C. (2004). Chemical characterisation of natural organic substrates for biological mitigation of acid mine drainage. *Water Research*, *38*(19), 4186–4196. https://doi.org/10.1016/j.watres.2004.06.023

Gozzard, E., Mayes, W. M., Potter, H. A. B., & Jarvis, A. P. (2011). Seasonal and spatial variation of diffuse (non-point) source zinc pollution in a historically metal mined river catchment, UK. *Environmental Pollution*, *159*(10), 3113–3122. https://doi.org/10.1016/j.envpol.2011.02.010

Harris, D. L., Lottermoser, B. G., & Duchesne, J. (2003). Ephemeral acid mine drainage at the Montalbion silver mine, north Queensland. *Australian Journal of Earth Sciences*, *50*(5), 797–809. https://doi.org/10.1111/j.1440-0952.2003.01029.x

Hashemian, S., Hosseini, S. H., Salehifar, H., & Salari, K. (2013). Adsorption of Fe(III) from aqueous solution by Linde Type-A zeolite. *American Journal of Analytical Chemistry*, *4*(7), 123–126. https://doi.org/10.4236/ajac.2013.47A017

Hedin, R. S., Narin, R. W., & Kleinmann, R. L. (1994). *Passive Treatment of Coal Mine Drainage* (Information Circular 9389). US Department of the Interior, Bureau of Mines.

Heidmann, I., Christl, I., & Kretzschmar, R. (2005). Sorption of Cu and Pb to kaolinite-fulvic acid colloids: Assessment of sorbent interactions. *Geochimica et Cosmochimica Acta*, *69*(7), 1675–1686. https://doi.org/10.1016/j.gca.2004.10.002

Hem, J. D., & Cropper, W. H. (1959). *Survey of Ferrous-Ferric Chemical Equilibria and Redox Potentials* (No. 1459-A). US Geological Survey.

Hengen, T. J., Squillace, M. K., O'Sullivan, A. D., & Stone, J. J. (2014). Life cycle assessment analysis of active and passive acid mine drainage treatment technologies. *Resources, Conservation and Recycling*, *86*, 160–167. https://doi.org/10.1016/j.resconrec.2014.01.003

Holub, M., Balintova, M., Pavlikova, P., & Palascakova, L. (2013). Study of sorption properties of zeolite in acidic conditions in dependence on particle size. *Italian Association of Chemical Engineering*, *32*, 559–564

Hydrometrics, Inc., & TKT Consulting, LLC. (2012). *Great Falls Coal Field Water Treatment Assessment* (303 p.). Montana Department of Environmental Quality, Helena, Montana.

Johnson, D. B., & Hallberg, K. B. (2005). Acid mine drainage remediation options: A review. *Science of The Total Environment*, *338*(1), 3–14. https://doi.org/10.1016/j.scitotenv.2004.09.002

Kefeni, K. K., Msagati, T. A. M., & Mamba, B. B. (2017). Acid mine drainage: Prevention, treatment options, and resource recovery. *Journal of Cleaner Production*, *151*, 475–493. https://doi.org/10.1016/j.jclepro.2017.03.082

Kepler, D. A., & McCleary, E. C. (1993). Successive alkalinity-producing systems (SAPS) for the treatment of acidic mine drainage. *Journal of American Society of Mining and Reclamation*, 195–204. https://doi.org/10.21000/JASMR94010195

Kruse, N. A., Mackey, A. L., Bowman, J. R., Brewster, K., & Riefler, R. G. (2012). Alkalinity production as an indicator of failure in steel slag leach beds treating acid mine drainage. *Environmental Earth Sciences*, *67*(5), 1389–1395. https://doi.org/10.1007/s12665-012-1583-5

Langmuir, I. (1918). The adsorption of gases on plane surfaces of glass, mica, and platinum. *Journal of the American Chemical Society*, *40*(9), 1361–1403. https://doi.org/10.1021/ja02242a004

Lee, T. R., & Wilkin, R. T. (2010). Iron hydroxy carbonate formation in zerovalent iron permeable reactive barriers: Characterization and evaluation of phase stability. *Journal of Contaminant Hydrology*, *116*(1), 47–57. https://doi.org/10.1016/j.jconhyd.2010.05.009

Li, L., Benson, C. H., & Lawson, E. M. (2005). Impact of mineral fouling on hydraulic behavior of permeable reactive barriers. *Ground Water*, *43*(4), 582–596. https://doi.org/10.1111/j.1745-6584.2005.0042.x

Limousin, G., Gaudet, J.-P., Charlet, L., Szenknect, S., Barthès, V., & Krimissa, M. (2007). Sorption isotherms: A review on physical bases, modeling and measurement. *Applied Geochemistry*, *22*(2), 249–275. https://doi.org/10.1016/j.apgeochem.2006.09.010

Liu, Y., Li, Y., Li, X.-M., & He, T. (2013). Kinetics of (3-Aminopropyl)triethoxylsilane (APTES) silanization of superparamagnetic iron oxide nanoparticles. *Langmuir*, *29*(49), 15275–15282. https://doi.org/10.1021/la403269u

Ludwig, R. D., McGregor, R. G., Blowes, D. W., Benner, S. G., & Mountjoy, K. (2002). A permeable reactive barrier for treatment of heavy metals. *Ground Water*, *40*(1), 59–66. https://doi.org/10.1111/j.1745-6584.2002.tb02491.x

Mayer, K. U., Benner, S. G., & Blowes, D. W. (2006). Process-based reactive transport modeling of a permeable reactive barrier for the treatment of mine drainage. *Journal of Contaminant Hydrology*, *85*(3), 195–211. https://doi.org/10.1016/j.jconhyd.2006.02.006

McMahon, P. B., Dennehy, K. F., & Sandstrom, M. W. (1999). Hydraulic and geochemical performance of a permeable reactive barrier containing zero-valent iron. *Ground Water*, *37*(3), 396–404. https://doi.org/10.1111/j.1745-6584.1999.tb01117.x

Moncur, M. C., Ptacek, C. J., Hayashi, M., Blowes, D. W., & Birks, S. J. (2014). Seasonal cycling and mass-loading of dissolved metals and sulfate discharging from an abandoned mine site in northern Canada. *Applied Geochemistry*, *41*, 176–188. https://doi.org/10.1016/j.apgeochem.2013.12.007

Motsi, T., Rowson, N. A., & Simmons, M. J. H. (2009). Adsorption of heavy metals from acid mine drainage by natural zeolite. *International Journal of Mineral Processing*, *92*(1), 42–48. https://doi.org/10.1016/j.minpro.2009.02.005

Nelson, J., Joe-Wong, C., & Maher, K. (2019). Cr(VI) reduction by Fe(II) sorbed to silica surfaces. *Chemosphere*, *234*, 98–107. https://doi.org/10.1016/j.chemosphere.2019.06.039

Nordstrom, D. K. (2009). Acid rock drainage and climate change. *Journal of Geochemical Exploration*, *100*(2), 97–104. https://doi.org/10.1016/j.gexplo.2008.08.002

Nordstrom, D. K. (2011). Mine waters: Acidic to circmneutral. *Elements*, *7*(6), 393–398. https://doi.org/10.2113/gselements.7.6.393

Nordstrom, D. K., Blowes, D. W., & Ptacek, C. J. (2015). Hydrogeochemistry and microbiology of mine drainage: An update. *Applied Geochemistry*, *57*, 3–16. https://doi.org/10.1016/j.apgeochem.2015.02.008

Obiri-Nyarko, F., Grajales-Mesa, S. J., & Malina, G. (2014). An overview of permeable reactive barriers for in situ sustainable groundwater remediation. *Chemosphere*, *111*, 243–259. https://doi.org/10.1016/j.chemosphere.2014.03.112

Pandová, I., Panda, A., Valíček, J., Harničárová, M., Kušnerová, M., & Palková, Z. (2018). Use of sorption of copper cations by clinoptilolite for wastewater treatment. *International Journal of Environmental Research and Public Health*, *15*(7), 1364. https://doi.org/10.3390/ijerph15071364

Parks, G. A. (1967). Aqueous surface chemistry of oxides and complex oxide minerals. In *Equilibrium Concepts in Natural Water Systems* (Vol. 67, pp. 121–160). https://doi.org/10.1021/ba-1967-0067.ch006

Puls, R. W., Powell, R. M., Paul, C. J., & Blowes, D. (1999). Groundwater remediation of chromium using zero-valent iron in a permeable reactive barrier. In *ACS Symposium Series*: *Innovative Subsurface Remediation* (Vol. 725, pp. 182–194). https://doi.org/10.1021/bk-1999-0725.ch013

Ramasamy, D. L., Khan, S., Repo, E., & Sillanpää, M. (2017). Synthesis of mesoporous and microporous amine and non-amine functionalized silica gels for the application of rare earth elements (REE) recovery from the waste water-understanding the role of pH, temperature, calcination and mechanism in Light REE and Heavy REE separation. *Chemical Engineering Journal*, *322*, 56–65. https://doi.org/10.1016/j.cej.2017.03.152

Ramasamy, D. L., Puhakka, V., Iftekhar, S., Wojtuś, A., Repo, E., Ben Hammouda, S., … Sillanpää, M. (2018). N- and O- ligand doped mesoporous silica-chitosan hybrid beads for the efficient, sustainable and selective recovery of rare earth elements from acid mine drainage: Understanding the significance of physical modification and conditioning of the polymer. *Journal of Hazardous Materials*, *348*, 84–91. https://doi.org/10.1016/j.jhazmat.2018.01.030

Rossillon, M., McCormick, M., & Hufstetler, M. (2009). *Great Falls Coal Field: Historic Overview* (104 p.). Mine Waste Cleanup Bureau, Montana Department of Environmental Quality, Helena, Montana.

Santomartino, S., & Webb, J. A. (2007). Estimating the longevity of limestone drains in treating acid mine drainage containing high concentrations of iron. *Applied Geochemistry*, *22*(11), 2344–2361. https://doi.org/10.1016/j.apgeochem.2007.04.020

Skousen, J., & Ziemkiewicz, P. (2005). *Performance of 116 passive treatment systems for acid mine drainage*. Presented at the 2005 National Meeting of the American Society of Mining and Reclamation, Breckenridge, Colorado.

Skousen, J., Zipper, C. E., Rose, A., Ziemkiewicz, P. F., Nairn, R., McDonald, L. M., & Kleinmann, R. L. (2017). Review of passive systems for acid mine drainage treatment. *Mine Water and the Environment*, *36*(1), 133–153. https://doi.org/10.1007/s10230-016-0417-1

Stumm, W., & Morgan, J. J. (1996). *Aquatic Chemistry: Chemical Equilibria and Rates in Natural Waters, 3rd ed*. Wiley & Sons. https://doi.org/10.5860/CHOICE.33-6312

Stylianou, M. A., Hadjiconstantinou, M. P., Inglezakis, V. J., Moustakas, K. G., & Loizidou, M. D. (2007). Use of natural clinoptilolite for the removal of lead, copper and zinc in fixed bed column. *Journal of Hazardous Materials*, *143*(1–2), 575–581.

Wang, S., & Peng, Y. (2010). Natural zeolites as effective adsorbents in water and wastewater treatment. *Chemical Engineering Journal*, *156*(1), 11–24. https://doi.org/10.1016/j.cej.2009.10.029

Watzlaf, G. R., Schroeder, K. T., & Kairies, C. L. (2000). Long-term performance of anoxic limestone drains. *Mine Water and the Environment*, *19*(2), 98–110. https://doi.org/10.1007/BF02687258

Yavuz, Ö., Altunkaynak, Y., & Güzel, F. (2003). Removal of copper, nickel, cobalt and manganese from aqueous solution by kaolinite. *Water Research*, *37*(4), 948–952. https://doi.org/10.1016/S0043-1354(02)00409-8

Zhu, M., Lerum, M. Z., & Chen, W. (2012). How to prepare reproducible, homogeneous, and hydrolytically stable aminosilane-derived layers on silica. *Langmuir*, *28*(1), 416–423. https://doi.org/10.1021/la203638g

Ziemkiewicz, P. F., Skousen, J. G., Brant, D. L., Sterner, P. L., & Lovett, R. J. (1997). Acid mine drainage treatment with armored limestone in open limestone channels. *Journal of Environmental Quality*, *26*(4), 1017–1024. https://doi.org/10.2134/jeq1997.00472425002600040013x

APPENDIX A

SUBSTRATES AND SURFACE MODIFICATIONS

For this investigation, various low isoelectric point substrates (sorbing surface, Tables A.1 and A.2) and surface modifications (metal capture enhancement, Tables A.1 and A.3) were evaluated for creation of a reactive substrate for insertion into the modular treatment system. The goal was to provide options for possible substrates that could be readily purchased and modified with potential ease of insertion/extraction into/from the treatment system. The focus of the substrate evaluation was selection of substrates that could capture Fe and other metals from solution through sorption or other secondary processes (e.g., mineral precipitation). Secondary processes of mineral precipitation or alteration of solution pH were not primary objectives of the substrate selection but provide additional metal capture properties that are composited into the overall evaluation of Fe removal from solution. The focus of the surface modification evaluation was to identify simple surface treatments that could enhance surface area availability and sorption properties. Additionally, chelators that could be readily applied to a possible substrate were evaluated to provide increased metal binding.

Table A.1: List and timeline of substrates and surface modification evaluated during this study.

Year:	2016	2017			2018				2019				
Quarter:	4	1	2	3	4	1	2	3	4	1	2	3	4
Substrate:													
S1	Steel plate												
S2	Tungsten wire												
S3	Silica felt/wool												
S4								Clinoptilolite					
Surface modification:													
SM1	Iron nanoparticle												
SM2	Carbon-coated iron nanoparticle												
SM3		Mesoporous silica nanoparticle											
SM4			Silica nanoparticle										
SM5			Cobalt nanoparticle										
SM6	Polyethylenimine												
SM7	(2-Aminopropyl)triethoxysilane												

A.1 Substrate summary

A hardened 1095 steel was initially examined as a sorbing surface that could be oxidized and magnetized for increased surface area and application of nanoparticles. Magnetization of the steel allowed for dip-coating of Fe-oxide nanoparticles with subsequent testing of chelator application. An off-the-shelf tungsten oxide wire was chosen as a preliminary substrate for testing of nanoparticle application and metal sorption because of the wire's low isoelectric point.

Stabilization of the tungsten wire surface by oxidation was tested by exposing the wire to aqua regia [HNO_3+3HCl], sulfuric acid [H_2SO_4], purified water, steam, and various concentrations of hydrogen peroxide [H_2O_2]. A silica felt/wool was chosen as a comparison substrate given a similarly low isoelectric point. Silica wool was initially wire-twirled for development of the support structure, but a rolled configuration proved to be an easier preparation method that produced similar permeability results. Clinoptilolite ($Na_6[Al_6Si_{30}O_{72}]24H_2O$), a naturally occurring zeolite, was introduced as an additional silicate substrate to be compared with silica wool (Si) and functionalized Si (Si+APTES). The atomic structure of zeolite offers large surface areas for sorption as well as loosely held cations (Ca, Mg, Na, K) readily available for cation exchange. Substrate experimental results indicated easier use and surface modification of Si and clinoptilolite. A final evaluation of Si+APTES and clinoptilolite allowed for a focused comparison of Fe sorption through batch and flow column sorption experiments described in this report.

Table A.2: Summary of surface properties and experimental results for substrates evaluated during this study.

ID	Material	Properties	Experimental Results
S1	Steel plate	• Magnetic surface for nanoparticle attachment • Can be oxidized for increased surface area	• Steel plates could not hold a magnetic charge
S2	Tungsten wire	• Negative surface charge for nanoparticles and/or sorption • Can be oxidized for increased surface area • pH_{pzc} suitable for ARD	• Surface preparation through oxidation provided substantial surface area • Oxidation/stabilization procedures were not reproducible • Surface modification inconsistent
S3	Silica felt/wool	• Negative surface charge for nanoparticles, chelator, and/or sorption • pH_{pzc} suitable for ARD.	• Stable under ARD conditions • Bare silica felt did not sorb iron under ARD conditions • Provided a surface for chelator application
S4	Clinop-tilolite	• Negative surface charge for chelator and/or sorption • pH_{pzc} suitable for ARD • High surface area, ion-exchanging properties	• Stable under ARD conditions • Raised pH from 3.0 to >6.0 temporarily • Removed iron through multiple processes • Easy surface preparation

A.2. Surface modification summary

An off-the-shelf carbon-coated, iron-core nanoparticle was selected as a preliminary surface modification for examination of solution interaction and plate-, wire-, and felt-coating applications. A Langmuir Blodgett was examined as a means of performing the nanoparticle application. The steel and tungsten substrates were dip coated at different nanoparticle concentrations and hold times following selection of an appropriate solution mixing procedure. An uncoated iron nanoparticle; a carbon-coated, cobalt-core nanoparticle; a mesoporous silica nanoparticle; and a silica nanoparticle were included in application tests to evaluate their potential for substrate surface modification. After several experiments, the carbon-coated, iron

core nanoparticle and the uncoated, iron nanoparticle produced the best coverage and sorption to the substrates compared to the other particles. The silica nanoparticle experienced massive clumping and poor attachment to the surface following application to the tungsten wire and exposure to water and acidic solutions. The mesoporous silica microparticles had an unexpectedly weak structure and broke apart during the application process, regardless of being in a low energy or high energy (sonicator application) environment. The cobalt nanoparticles behaved similarly to their iron-core counterpart, but are more expensive. Some experiments yielded excellent nanoparticle coverage (distribution) that was previously unseen on tungsten wire that were not oxidized, but repeatability of widespread nanoparticle surface coverage under oxidized conditions was an issue. A mixture of carbon-coated iron nanoparticles (CFeNP) and(or) (3-Aminopropyl)triethoxysilane (APTES) concentrations were applied to various configurations of the silica felt/wool substrate in an attempt to optimize the substrate modification procedure. Substrate samples were analyzed through sorption tests (Fe removal efficiency) and comparison of substrate images with use of the scanning electron microscope. The application of iron nanoparticles (CFeNP) to silica fibers (Si) proved consistently difficult. Additionally, sorption experiments showed no evidence that Si+CFeNP+APTES substrates remove greater amounts of Fe^{2+} than Si+APTES substrates. The functionalization procedure for APTES has a simplicity of application in comparison to other potential chelators such as polyethylenimine (PEI) or Ethylenediaminetetraacetic acid (EDTA). Nanoparticle and chelator application using an ethanol solution were consistently equal or greater to coverage produced with a decane or toluene carrier solution.

Table A.3: Nanoparticle and chelator types, properties, and experimental results for surface modifications examined during this study.

ID	Material	Properties	Experimental Results
SM1	Iron nanoparticles (FeNPs)	• Increases surface area • Can be functionalized with a chelator	• Poor surface coverage and clumping in areas
SM2	Carbon-coated, iron nanoparticles (CFeNPs)	• Increases surface area • Can be functionalized with a chelator • Carbon coating reduces clumping	• High surface coverage • Carbon coat prevented significant clumping • No significant increase in iron sorption
SM3	Mesoporous silica nanoparticles (MSiNPs)	• Increases surface area • Can be functionalized with a chelator	• Low surface coverage • Destruction of mesoporous structures with application
SM4	Silica nanoparticles (SiNPs)	• Increases surface area • Can be functionalized with a chelator	• Poor surface coverage • Severe clumping • Loss of coverage when exposed to water
SM5	Carbon-coated, cobalt nanoparticles (CCoNPs)	• Increases surface area • Can be functionalized with a chelator • Carbon coating reduces clumping	• Low surface coverage • Carbon coating prevented significant clumping
SM6	Polyethylenimine (PEI)	• Chelator • High viscosity • High metal binding	• Silanization procedure difficult due to high viscosity • Low surface coverage • Insignificant Fe chelator under ARD conditions
SM7	(3-Aminopropyl) triethoxysilane (APTES)	• Chelator • Low viscosity • High metal binding	• Silanization of silica felt proved to be a simpler procedure than with PEI • 2% APTES, 98% ethanol solution ideal for application • High surface coverage • Effective Fe chelator under ARD conditions

A.3 Substrate and surface modification examples

Following are examples of tested substrates and surface modifications described in the previous sections of Appendix A.

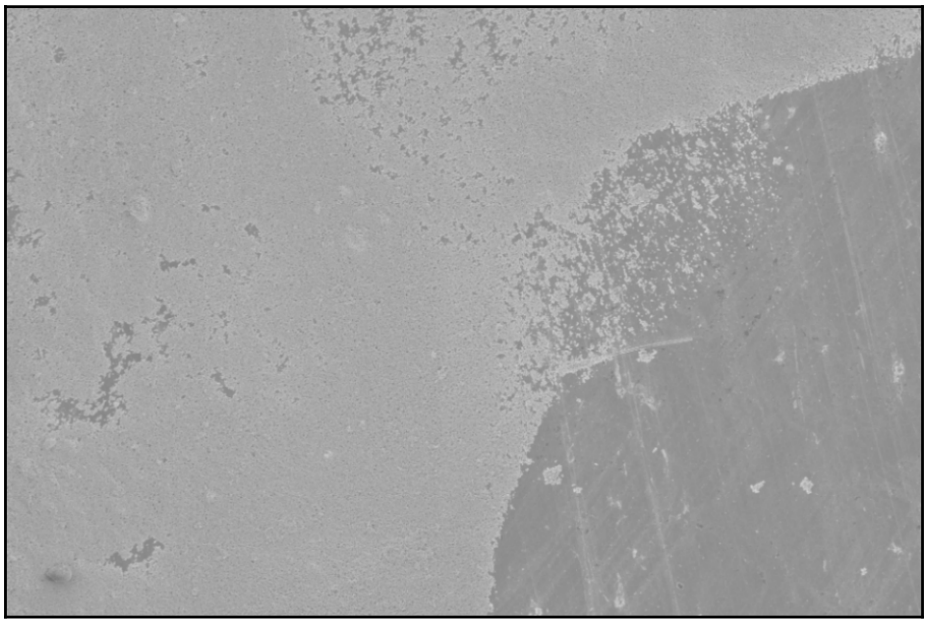

Figure S1: Steel plate (dark gray) magnetized and coated with FeNPs (SEM, 300×). Steel plate magnetized with a copper wire and dipped into a solution of FeNPs suspended in methanol. Steel plates could not hold a magnetic charge for longer than a week.

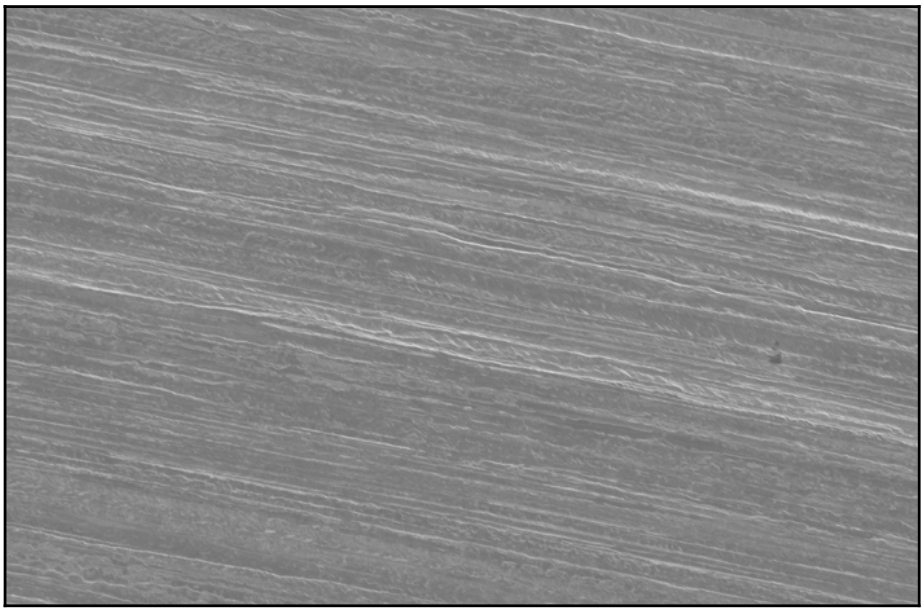

Figure S2a: Unoxidized tungsten wire prior to surface modification (SEM, 2,000×).

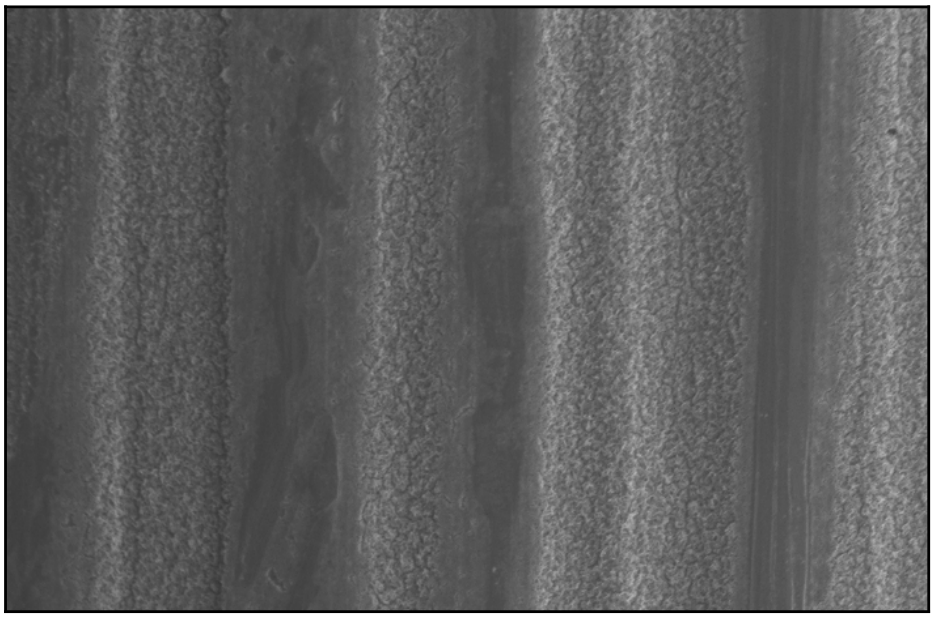

Figure S2b: Oxidized tungsten wire showing signs of pitting (corrosion) (SEM, 2,000×). Tungsten wire soaked in sulfuric acid solution for three days, followed by storage in ultrapure water for three days to stabilize the surface and provide additional surface area for nanoparticle coverage.

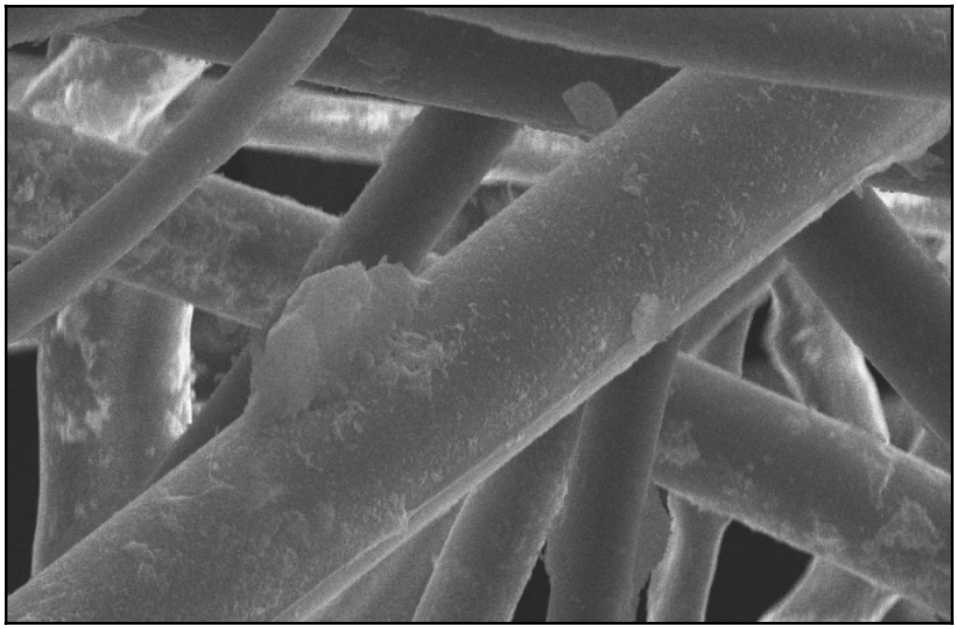

Figure S3: Silica felt with starch coating (light gray topography) prior to surface modification (SEM, 1,640×). Starch coating applied by manufacturer to provide rigidity for easier handling.

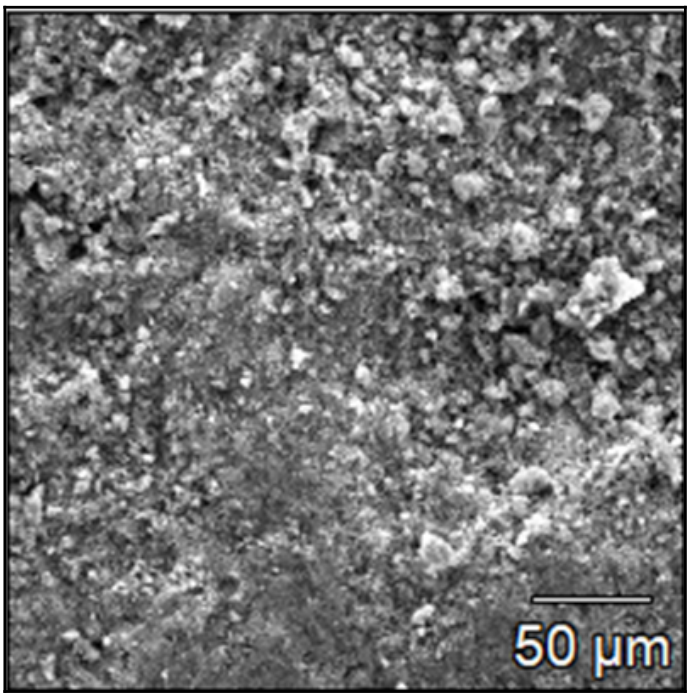

Figure S4: Clinoptilolite surface showing variable topography (SEM, 380×). High surface area, negative surface charge, and ion-exchanging properties allows clinoptilolite to sorb metals.

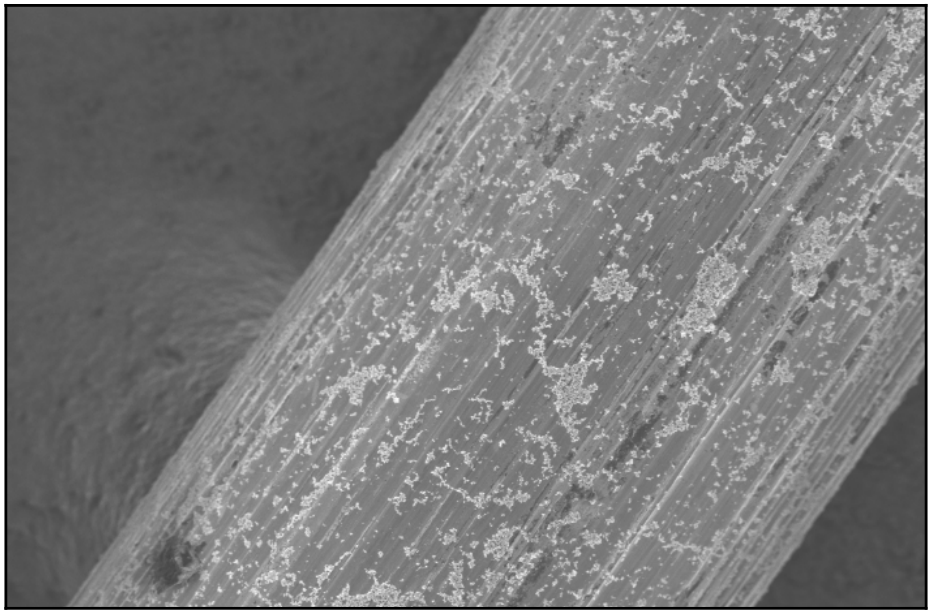

Figure SM1: Uneven coverage and clumping of FeNPs (light gray particles) on oxidized tungsten wire (SEM, 300×). Oxidized tungsten wire suspended in sonicated FeNP and decane solution for 10 min.

Figure SM2: Even coverage of CFeNPs (light gray particles) on oxidized tungsten wire (SEM, 2,000×). Oxidized tungsten wire suspended in sonicated CFeNP and decane solution for 10 min.

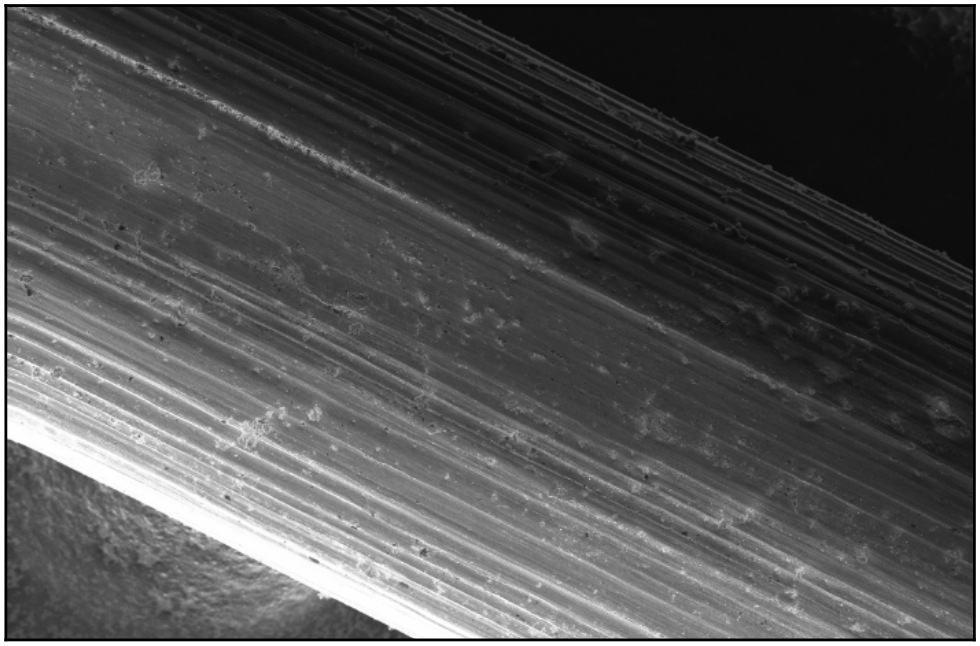

Figure SM3: Low surface coverage of MSiNPs (light gray particles) on oxidized tungsten wire (SEM, 300×). Oxidized tungsten wire suspended in MSiNP and ultrapure water solution for 10 min.

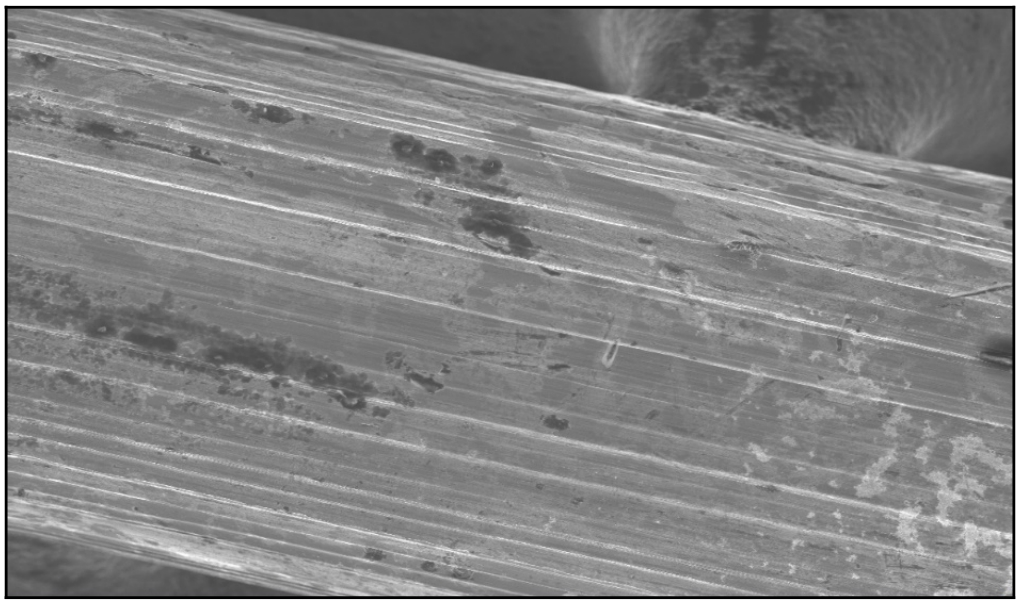

Figure SM4: Low surface coverage of SiNPs (light gray particles) on oxidized tungsten wire (SEM, 300×). Oxidized tungsten wire suspended in SiNP and ultrapure water solution for 10 min.

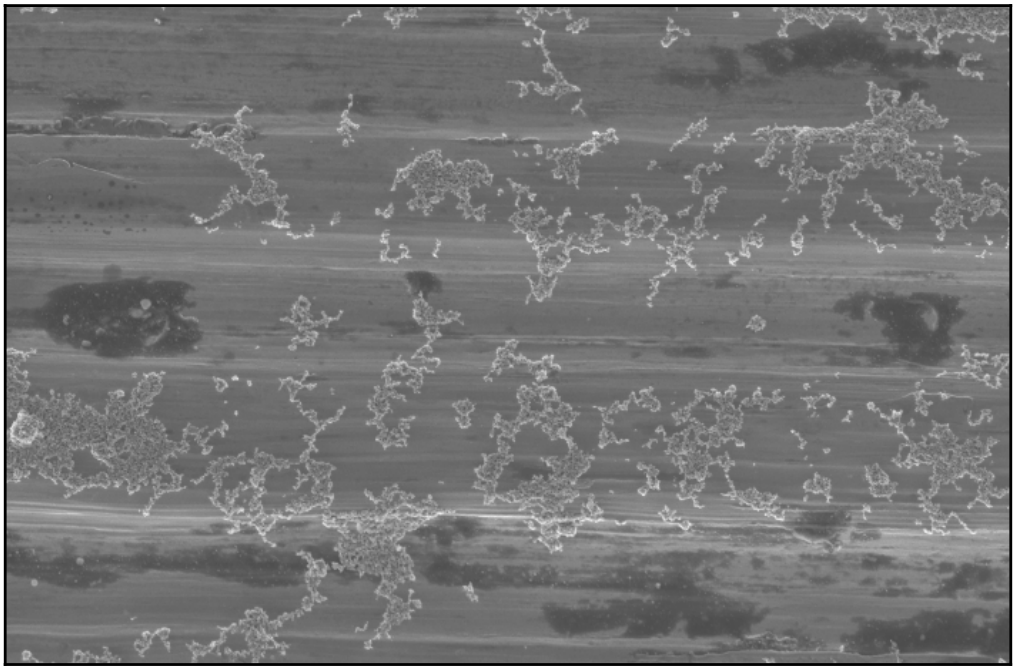

Figure SM5: Low surface coverage of CCoNPs (light gray particles) on oxidized tungsten wire (SEM, 300×). Oxidized tungsten wire suspended in sonicated CCoNP and decane solution for 10 min.

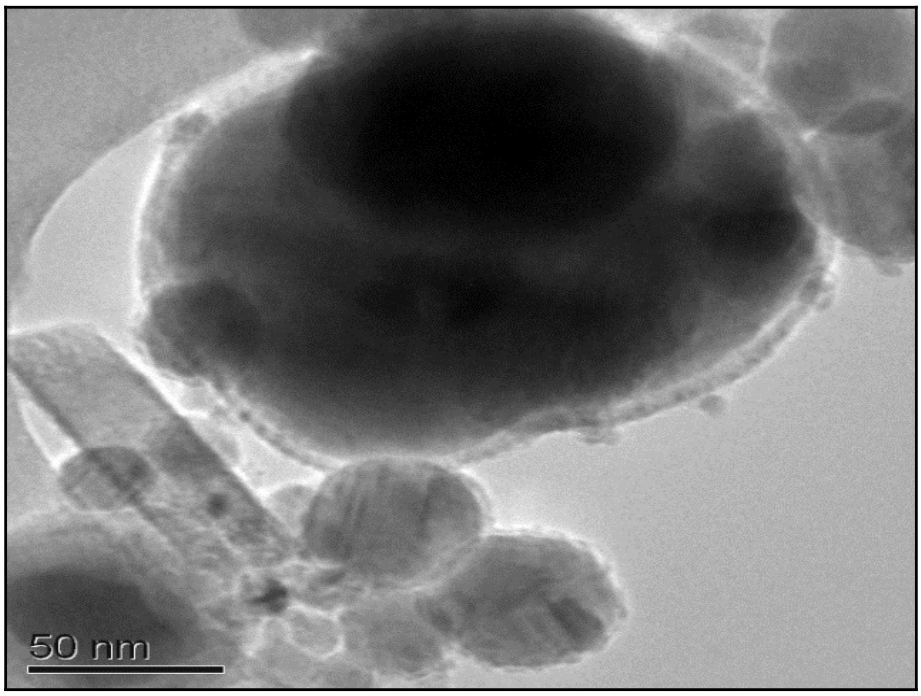

Figure SM6: Low surface coverage of PEI (light gray topography) on the surface of CFeNPs (larger dark gray spheres) (TEM, 60,000×). CFeNPs suspended in sonicated PEI and ethanol solution for 10 min.

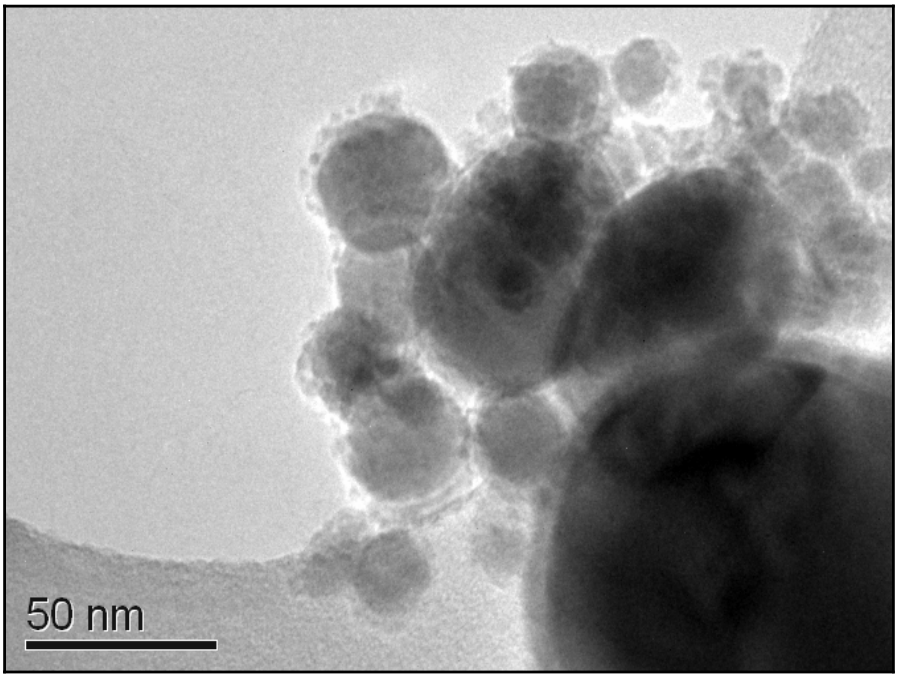

Figure SM7: High surface coverage of APTES (light gray topography) on the surface of CFeNPs (larger dark gray spheres) (TEM, 60,000×). CFeNPs suspended in sonicated APTES and ethanol solution for 10 min.